Shock Dynamics Laboratory
Department of Physics
Washington State University
Pullman, Wa. 99163

Internal Report 73-04

TO: Shock Dynamics Group

FROM: G. E. Duvall

DATE: May 4, 1973

Chapter 9 From
Dynamic Response of Materials to
Intense Impulsive Loading
P. C. Chou & A. K. Hopkins, eds.

TA
407 in Owen Library
C6

Chapter IX -- Applications

9.1 Introduction

Applications of the mechanics and physics of impact are extremely wide ranging. They extend throughout science and into much of engineering; they have widespread commercial implications; they are natural accompaniment to the violence associated with war. Military needs have led to development of much of the understanding of impact processes, but presently the importance of constructive applications in science and technology may exceed that of the military. A few applications of various kinds are described here in some detail and others are mentioned. To do more would require a separate text. References for further reading are given where possible, but unfortunately much of the material on applications is buried in non-public files.

9.1.1 Detonation

Earlier chapters of this book have not dwelt on the properties of explosives and the detonation process. Since many applications of dynamic loading are inseparable from detonation, a brief description will be given here.

A detonation wave is a shock in a chemically reacting material. Passage of the detonation shock through such a material increases pressure and temperature to the reaction point; reaction proceeds to completion in a sonic region behind the shock front and is followed by a rarefaction wave in the detonation gases. Detonation is very different from combustion. The latter propagates subsonically through the combustible mixture, and the pressures generated are not large, except through the effects of the confining container. Most of the explosions occurring in industrial accidents are due to confined combustion, e.g. dust explosions. But nitroglycerine, dynamite, PETN, RDX, etc. detonate. Their destructive effects are not substantially altered by confinement.

A simple and rather effective model of detonation is the Chapman-Jouguet model. It is not physically exact but is a good first approximation for calculating detonation pressures and other properties. The detonation front is assumed to be discontinuous in pressure, temperature, etc., and the detonation reaction is assumed to take place in a zone immediately behind the shock front. Flow is assumed to be sonic at the plane where chemical reaction is complete:

$$u_1 + c_1 = D \tag{9.1}$$

where subscripts "1" denote values at the end of the reaction zone and D is detonation velocity. If the detonation gases satisfy an Abel equation of state [9.1]:

$$p = NRT\rho/(1 - a\rho) , \tag{9.2}$$

Eq. (9.1) can be combined with the jump conditions to provide the following relations at the Chapman-Jouguet plane, i.e., the plane where Eq. (9.1) applies:

$$\rho_0/\rho_1 = (\gamma + a\rho_0)/(1 + \gamma) \tag{9.3}$$

$$u_1/D = (1 - a\rho_0)/(1 + \gamma) \tag{9.4}$$

$$c_1/D = \rho_0/\rho_1 \tag{9.5}$$

$$p_1 = \rho_0 D^2(1 - a\rho_0)/(1 + \gamma) \tag{9.6}$$

$$D^2 = 2(\gamma^2 - 1)Q/(1 - a\rho_0)^2 \tag{9.7}$$

$$p_1 = 2\rho_0(\gamma - 1)Q/(1 - a\rho_0) \tag{9.8}$$

where subscript "o" refers to the undisturbed state, γ is the ratio of specific heats, a is "co-volume" of the gases and Q is heat of reaction at V_o, p_o. p_1 is called the "Chapman-Jouguet pressure" of the explosive. To a good approximation many solid explosives satisfy an ideal gas equation of state with $a = 0$

and $\gamma \approx 3$ [9.2]. Some properties of commonly used explosives are given in Table 9.1.

Table 9.1

Properties of Some Common Explosives*

Explosive	p_1, kbar	u_1, mm/μsec	D, mm/μsec	ρ_0, g/cc	ρ_1, g/cc	γ
RDX	338	2.21	8.64	1.767	2.375	2.90
TNT	189	1.66	6.94	1.637	2.153	3.17
64/36-RDX/TNT (Comp. B)	292	2.13	8.02	1.713	2.331	2.77
77/23-RDX/TNT (Cyclotol)	312	2.17	8.25	1.743	2.366	2.80

*W. E. Deal, J. Chem. Phys. 27 (Sept. 57), 796-800.

Isentropic expansion from the Chapman-Jouguet state is determined by combining the equation of an isentrope,

$$p(V - a)^{\gamma} = \text{constant} , \tag{9.9}$$

with the Riemann integral

$$u - u_1 = \pm \int_{p_1}^{p} dp/\rho c .$$

The result is

$$u - u_1 = 2[\gamma p_1 (V_1 - a)]^{1/2} [(p/p_1)^{(\gamma-1)/2\gamma} - 1]/(\gamma-1). \tag{9.10}$$

A shock wave running into the Chapman-Jouguet state satisfies a (p,u) relation

$$(u - u_1)^2 = 2(p-p_1)^2 (V_1-a)/[p(\gamma+1) + p_1(\gamma-1)]. \tag{9.11}$$

The pressure induced in an inert solid by a plane detonation wave normally incident on the interface is determined by the intersection of the (p,u) curve for

a backward facing wave in the explosive, obtained from Eqs. (9.10) and (9.11), with the Hugoniot of the inert. Some examples are given in Fig. 9.1.

The Chapman-Jouguet state in an explosive is always followed by a rarefaction [9.3], so the shock wave induced in a sample is not followed by a uniform state. However, the uniform state can be approached very closely by making the explosive pad very thick (cf. Chapter 8). In this case it must also be made very large in diameter, so the amount of explosive involved increases as the cube of the significant experimental dimension.

9.2 Scientific Applications

These are extremely varied and few have been investigated in great depth. Reasons for the importance of shock studies in science are two-fold: the shock wave provides a relatively easy method for producing very high pressures and reasonably large compressions. Since pressure has some influence on all material properties, it is natural to try to explore such effects. Secondly, the very rapidity with which stress is applied in the shock process represents a variation from the usual scientific experiment, which is static or quasistatic at best, and it is a matter of great interest to determine whether or not laws of physical behavior inferred from such experiments can be reliably extrapolated to dynamic situations. The techniques and principles outlined in earlier chapters can be combined to yield the results that rate effects between about 10^5/sec and 10^8/sec can be investigated in shock experiments and that phenomena which equilibrate in a microsecond or less can be studied under essentially equilibrium conditions.

9.2.1 Solid State and Materials Science

Problems which have been studied under shock conditions include equations of state, electrical and magnetic properties, interatomic potentials, hardening of metals, phase transitions, dynamics of mechanical failure and constitutive relations. We shall examine particularly phase transition measurements.

The most notable success in the study of phase transitions by shock wave techniques is the discovery of the transition from body centered cubic to the hexagonal close packed phase in iron at 130 kbar by Minshall in 1954 [9.4]. It was thought to be a transition to the well known face-centered cubic phase (γ) of iron until 1961 when Johnson, Stein and Davis [9.5] showed by shock techniques that the P-T phase line is thermodynamically inconsistent with transition to the γ phase. Identification of this hitherto unknown phase was accomplished by x-ray diffraction studies at high static pressure, directly stimulated by the shock wave experiments. This initial foray into the study of pressure-induced phase

transitions has led to excursions and to some unanswered questions about the mechanisms of rapidly occurring transitions.

Some equilibrium p-V curves for a first order solid-solid phase transition are shown in Fig. 9.2. OAB is an isotherm for which $(\partial p/\partial V)_T = 0$ in the mixed phase region. OCD is the isentrope through O. Point C is a cusp with a discontinuity in slope; $(\partial p/\partial V)_S < 0$ on CD, but not by much. OEF is the Hugoniot centered at O. It too has a cusp at the phase boundary, and if the final shock pressure is greater than p_1 but less than p_2, two shocks are formed. Above p_2 a single shock is stable.

Two procedures can be used to detect shock-induced phase transitions: one is to drive the shock with final pressure between p_1 and p_2 so as to produce a double wave. The amplitude of the first wave, ignoring the elastic precursor, is then the stress for transition. If measurements made on samples of different thickness show no change in the first wave amplitude, it is presumed to be equal to the stress of static transition. It means, more precisely, that the rate of transition at this pressure is too slow (or too fast) to be detected in the experiment. Experience has indicated that, very often at least, it is the static transition pressure.

The second procedure is based on cruder experimental techniques, but is nonetheless effective. The "flash gap" technique, described in Chapter 8, is indifferent to the presence of multiple waves. From each experiment only a single shock arrival is recorded, corresponding to the transition pressure. If a graph is made of U_s vs U_p, as in Fig. 9.3, a region is found in which U_s remains constant while U_p increases. This corresponds to the region between p_1 and p_2 in Fig. 9.2 in which only the first shock arrival is recorded. Because p is not varied continuously, it often happens that the plateau in U_s is not observed; there is only a break in slope in the U_s-U_p diagram, and this break in slope is taken to be the transition pressure. The technique is limited

in accuracy by spacing of the experimental points. Materials in which phase transitions have been studied by shock techniques include iron and its alloys [9.7], various rocks and minerals [9.8], bismuth [9.9], germanium [9.6], various alkali halides [9.10] and numerous other materials [9.11]. A particularly interesting shock-induced transition is that from graphite to diamond. The mechanics of this are not understood. The transition pressure lies between 100 and 1000 kilobars, depending on the initial density of the graphite, and the recovered diamonds are polycrystalline particles, most of which are a few microns or tens of microns in diameter, composed of crystallites the order of a few hundred angstroms diameter [9.12].

One of the effects of phase transitions is to change the conductivity of the material. There has long been an interest in the metallic phase of hydrogen and calculations of the transition pressure range from less than one to the order of twenty megabars. Such a transition is not apt to be achieved in shock waves, but other transitions from molecular to atomic forms should exist, as in the halogens, and may well be accessible to shock wave experiments.

9.2.2 Geophysics

Geophysicists have responded eagerly to the availability of shock wave techniques for study of high pressure and impact phenomena. This response is due to interest in composition of the earth and its core, where pressures exceed three thousand kilobars, and in the properties of meteor craters, which are produced by very high speed impact.

The problem of earth composition is to determine combinations of materials which are naturally abundant and geologically probable and which reproduce the average density of the earth, its moment of inertia, and measured variations of seismic wave velocity with depth [9.13]. The increase of temperature with pressure in the interior of the earth is thought to resemble that occurring in shock compression of rocks, so Hugoniot data can be compared directly with model

values[9.14]. Such comparisons have led to the conclusion that an iron-silicon mixture is compatible with composition of the earth's core, and that the mechanical properties of olivine, a mixture of magnesium and iron silicates, are compatible with known properties of the upper mantle [9.8], [9.14].

A very recent and exciting development is the discovery that shock compression of rocks produces permanent changes which can be used as shock indicators when studying the microscopic properties of terrestrial, lunar or other rocks. This field, which has grown rapidly, is now known as "shock metamorphism."

After development of a space program in the United States, following the launching of the first Sputniks in 1957, the attentions of rather large numbers of scientists were turned for the first time to close consideration of characteristics of other planets in our own solar system and of our moon. Among questions which received particular attention is that which concerns the role played by meteoritic impact in determining the surface structure of the moon: to what extent are visible craters on the moon due to meteorite impact rather than, say, volcanism? These questions led, in turn, to more detailed consideration of the physical consequences of meteoritic impact, then to studies of shock effects on rocks and minerals, and finally to the realization that the best source of information on this subject may lie on our own earth. If we can understand the extent to which meteoritic impacts have influenced surface structure of the earth we may be able to understand the surface of the moon and rely on moon missions only for confirmation of the theory.

Through studies on rocks from craters, which began in 1872, and recent experiments using shocks from nuclear and chemical explosions, certain characteristic features of rocks have been reasonably well established as being due to the passage of shock waves [9.15]. These features are different for iron and for stony meteorites. The majority of meteorites found and identified on earth are

iron, for obvious reasons: an iron meteorite is malleable and is apt to stay in one piece during and after impact. Stony meteorites shatter and mingle with the surrounding natural rocks. It is therefore quite possible that the bulk of meteorites striking the earth are stony, but unidentified.

The minimum velocity with which a meteorite originating within our solar system may enter the earth's atmosphere is about eleven mm/μsec. Assuming the meteorite to enter the atmosphere with minimum velocity, to be spherical with radius r and density ρ, no mass to be lost by erosion, and a uniformly dense atmosphere, we find its velocity at the surface of the earth to be approximately 11 $\exp(-375\ \alpha/\rho r)$ where α is drag coefficient, approximately equal to unity for supersonic velocities[9.16]. Iron meteorites of 5 cm radius or less should reach the earth at their terminal velocities in free fall, about 7500 cm/sec. Smaller meteorites will slow more or burn, larger meteorites will slow less. Velocities of some larger meteorites at the surface of the earth, assuming they have entered the atmosphere at eleven mm/μsec are given in the ~~following~~ table 9.2.

TABLE 9.2
Velocities of Iron Meteorites
at the Earth's Surfaces

radius, cm:	10	15	20	30	50	100
velocity, cm/sec:	9400	4.6×10^4	10^5	2.26×10^5	4.3×10^5	6.8×10^5

Iron striking anorthosite at .095 mm/μsec produces a shock of about 10 kb. At 1.0 mm/μsec, the impact pressure is 120 kb and at 5 mm/μsec it is 800 kb. For stony meteorites the pressure corresponding to the same impact velocity will be 50 to 70% of values obtained with iron. So a great range of shock pressures, extending to over a 1000 kilobar, can be expected in various meteoritic impacts. Physical changes in rocks and minerals subjected to such impact are high pressure effects, such as phase transitions, high strain rate effects involving the

restructuring of grains and crystallites, and high temperature effects, primarily melting[9.15].

In iron meteorites, which are composed of α and γ iron, nickel, carbon, FeS, Fe_3P, Fe_3C and traces of other materials, shock indicators are very prominent. They include "widmanstätten" patterns, attributable to the 130 kb α-ε transition in iron, recrystallization above about 600 kb and formation of martensite or pearlite from shock heating. The FeS changes crystallite size and orientation and may melt under strong shock. Fe_3C recrystallizes and carbon may appear as both graphite and shock-induced diamond. The latter consists of crystallites of a few hundred angstroms diameter bound into aggregate particles a few tenths millimeter in diameter[9.17].

Identification of craters produced by stony meteorites is more difficult than for iron meteorites and depends to a large extent on microscopic analysis of materials collected from the crater. General features of a crater are its circularity and certain characteristic folding and faulting, together with "brecciation" of fine material, i.e., compaction of loose soil into rock[9.15]. "Shatter cones" may be present. These are cone-shaped pieces of rock showing evidence of brittle fracture on their surfaces and believed to be formed by passage of shock waves and subsequent rarefactions through large rock structures. Microscopic studies reveal the presence of coesite and stishovite, these being high pressure forms of quartz, and of quartz grains containing lamellae similar to crystallographic twins. The presence of maskelynite is common, this being an isotropic form of feldspar. Selective melting of mineral constituents and the presence of glassy fragments are also observed. By these means, understanding of the role of meteoritic impact on earth surface structure has been greatly expanded since 1960 when coesite was discovered. This is illustrated by Fig. 9.4, which shows the number of identifiable craters discovered since 1925. Some recently identified

craters are the order of 30 miles in diameter, and it has been suggested that major features such as the Gulf of St. Lawrence and Hudson Bay Arc may even be of meteoritic origin[9.15].

Since return of the Apollo 11 and 12 missions there has been intense study of the lunar rocks collected. The lunar surface appears to be composed largely of fine dust to considerable depth with outcroppings of solid rocks on the heights[9.18]. There is strong evidence of meteoritic impact in the form of brecciation and melting. Few lamellar markings in quartz or other indicators of intermediate shock have been found; the overwhelming evidence is from melting[9.19].

9.2.3 Miscellaneous

The principal application of shock wave and impact techniques in solid state chemistry is to the initiation of detonation. These studies have been motivated primarily by safety considerations and only in recent years by desire and need to know more about the process of initiation itself. Explosives have been beaten by hammers, crushed by falling weights, dragged over rough surfaces, dropped on the decks of battleships, drilled, poked, squeezed, pressed, burned, and otherwise mistreated, all in the interests of safety. The result is that an extensive lore of initiation has developed with very little real understanding. In the 1950's there started various experiments designed to shed some light on the mechanical and chemical processes involved in initiation. These have taken various forms, but have all been intended to expose the solid explosive to a plane shock wave for a known time and to determine the extent of reaction which occurred.

An experimental arrangement designed to measure the initiation of detonation by a sustained shock is shown in Fig. 9.5a. The flyer plate is accelerated across a gap by an explosive system and strikes one face of an explosive

sample. The arrival time of the flyer at the left surface of the sample is recorded by pins "A"; arrival of the detonation wave at the right surface of the sample is recorded by pins "B." The difference between these times, $T_B - T_A$, is the transit time through the sample, T. The thickness of the sample, d, and its steady detonation velocity, D, are known. The quantity $t = T - d/D$ is called the "excess transit time" and is a measure of the time required to start a steady detonation for the particular shock generated by this impact. A "time to detonation" can be defined as

$$t_b = D\, t/(D - \bar{U}_s)$$

where $\bar{U}_s$ is a mean value of shock velocity in the sample. The results of such a set of experiments are shown in Fig. 9.6 for a particular explosive mixture known as HMX 9404-03 [9.20]. As the flyer plate velocity increases, the time required to initiate detonation decreases. A difficulty encountered in interpreting such experiments is that the Hugoniot of the unreacted explosive is generally unknown [9.21].

When the thick plate is replaced by a thin foil, as in Fig. 9.5b, the excess transit time, t', is greater than t. The effect is shown in Fig. 9.7. It seems clear that obtaining information of this kind represents a step toward understanding of these particular solid state reactions. It seems equally clear, however, that quantitative understanding is far off, particularly when the likelihood of three-dimensional effects influencing even plane detonations is considered [9.22].

Another interesting application is to the production of very high magnetic fields [9.23]. This is accomplished by first establishing a large static field in a configuration containing a short circuited conductor, then explosively accelerating the conductor. Magnetic flux, which is equal to the product of magnetic induction and area, remains constant through the induction of eddy currents, area diminishes, so magnetic induction increases. Fields the order of 10^7 gauss have been generated in this way.

9.3 Engineering and Commercial Applications

These include explosive forming and welding, impact sintering of granular materials, explosive devices such as bolts, switches, timers, detonators, and electrical pulse generators, demolition and construction techniques for moving and fracturing rock, synthesis of new materials, such as diamond and BN, impact drilling, etc.

9.3.1 Impact Bonding

Explosive welding is a major area of application of impact mechanics. It was initially suggested by knowledge that metals can be permanently bonded under static pressure if two clean surfaces are brought together under high pressure and held for long enough to allow diffusion to take place. It seemed reasonable to suppose that the high pressures produced by high velocity impact might serve to produce diffusion welds, even though the available time at pressure is small. It has in fact turned out to be quite easy to produce impact welds, though the mechanisms are not well understood.

The nature of the impact welding process is such that material is removed from the bonded surfaces during impact so prior cleansing is not required. Bonding is accomplished most readily in the configuration illustrated in Fig. 9.8 [9.24]. The two metals to be bonded are inclined at an angle α. If the velocity of the point of impact as it sweeps across the plates is supersonic, a steady shock configuration originates at the impact point and flow in both materials is stable. Bonding occurs most readily if the velocity is subsonic, a condition achieved by adjusting α. Then flow is unstable about the impact point and stress waves run ahead in one metal or both. One manifestation of unstable flow in this configuration is jetting [9.25] and theories of welding have been based on this hypothesis [9.26], [9.27]. Bonding may be produced whether air is allowed between the plates or not. If the system is evacuated the welds are

more uniform and can be formed at lower impact velocities. The minimum impact velocities at which aluminum can be welded to aluminum and copper to copper are .12 mm/μsec and .23 mm/μsec respectively. Some micrographs of explosively-bonded specimens using the above technique, with subsonic flow, are shown in Fig. 9.9. Ripple marks at the interface are characteristic of the impact bond, but are occasionally absent. The scale of ripples is determined by the materials involved, impact velocity and impact angle.

Principal difficulties encountered in applying the above technique to commercial processes are in setting the pieces at an angle $\alpha > 0$ and in evacuating the space between them. Both these problems can be avoided by placing the metals in loose contact and compressing them with an explosive which has a detonation velocity less than the elastic velocity in either metal. If the explosive is detonated at one end, the detonation, and therefore the point of impact, sweeps across the metal interface subsonically, thus satisfying the conditions for unstable flow.

There still remain many questions to be answered concerning the mechanics of impact bonding, but these do not prevent its application; it is presently being used, for example, to produce nickel-clad copper used in U.S. coins. It has been reported that bonding can be achieved between two plates in contact using sufficient explosive of high detonation velocity even though the subsonic condition is violated [9.28]. And the occasional formation of butt welds between adjacent pieces overlaid with explosive has also been reported [9.29]. In neither case are the conditions for unstable flow satisfied.

9.3.2 Shock Synthesis of Diamond

One of the most fascinating commercial or near-commercial applications of shock generation procedures is synthesis of diamonds from

graphite [9.30]. There has been speculation about the synthesis of diamond in explosive assemblies for a very long time, and it is quite possible that some early experiments actually succeeded in producing diamonds, though positive identifications were not possible [9.31]. The first successful, verified effort was reported by De Carli and Jameson in 1961 [9.12]. The principal problem they encountered was not in the making of diamond, that turned out to be quite easy; but rather in its separation from the graphite in which it was formed. Individual crystallites were found to be the order of a hundred Angstroms in diameter, so rather high concentrations are necessary before positive identification can be made by x-ray diffraction. A phase diagram for diamond, which is quite speculative, is shown in Fig. 9.10. The shaded region labeled "shock wave synthesis region" represents the range of shock pressures and temperatures in which De Carli has succeeded in producing diamonds. In these experiments temperature and pressure variations are associated with variations in the shock driver system and in initial graphite density. Graphite can be shocked either by placing explosive in direct contact with graphite or a container of graphite or by using explosive to drive a flyer plate against graphite or graphite container. When graphite density is increased in a given explosive system, shock pressure usually increases but shock temperature may go down. Introduction of porosity in a sample at fixed shock pressure causes temperature to increase rapidly. Because of this interdependence of temperature, pressure and porosity, it is a difficult matter to determine the (P,T) region in which shock synthesis occurs. The situation is further complicated by variations in duration of shock pressure in various experiments. By and large it can be said that duration of the shock pulse diminishes as amplitude increases. Then if the transformation from graphite to diamond is a rate process, the rate of transformation diminishes as temperature decreases. So the amount of transformation which occurs in a given experiment may diminish as the pressure increases.

Moreover, there is most likely some reversal of the transformation on release of shock pressure. De Carli reports [9.32] some indication that shock synthesized diamond which has been allowed to cool slowly after being shocked contains larger crystallites than samples which are rapidly quenched. This seems rather odd, since graphite is the stable phase at atmospheric pressure; it is one more indication that shock synthesis of diamond is a very complicated process and that our understanding of it is still very limited.

Before any reader rushes out with explosive and graphite to manufacture a diamond bauble for his lady, he should be warned that the product is blackish or silvery, very hard to separate from graphite, polycrystalline, and very small. Some of the larger ones are shown in Fig. 9.11.

Shock wave synthesis of valuable materials may turn out to be a fruitful area for application of shock wave technology. It is difficult to assess the present commercial status of shock-synthesized industrial diamonds, but at least two companies are involved in the process and presumably hope that it will be profitable. There may be other substances which can be synthesized this way which will prove to be equally or more profitable; very small particles of cubic boron nitride have been produced in shock, and other candidates may appear.

9.4 Ordnance Applications

The fundamental processes of war are destruction of property and personnel and protection from destruction. Of various destructive processes which exist or can be invented, destruction by violent mechanical means is certainly most common; and this leads directly to problems of impact and shock wave propagation. It has been emphasized in previous pages that applications of shock wave studies are not limited to the military, but there is no denying that they are important to military matters. Many ordnance applications are obvious and well known. Other applications are newer and may relate to subjects discussed earlier in this chapter. Impact considerations are involved in penetration of armor plate, fragmentation of shells, acceleration of particles by explosives, explosive dispersal of liquids, blast effects of explosives and demolition, nuclear weapon design and many other problems. Here we consider design of liquid dispersal devices and armor penetration.

9.4.1 Explosive Dispersal of Liquids

An idealized version of an explosive device for dispensing liquids is shown in Fig. 9.12. The central sphere, region 0, contains explosive, the spherical shell, A, separates material to be dispersed, in B, from explosive, and the outer shell, C, encases the device. Practical details, such as placement of the initiator and its leads are ignored. In the ideal case the explosive, 0, is initiated at the center and a spherical detonation wave travels outward. Impinging on the shell A, it produces a series of shocks which are transmitted to the filler, B. These shocks tend to coalesce by the usual shocking-up process as they move outward, and a single shock will normally impinge on the outer case material, C. There will usually be a shock reflected into B from C and one driven forward into C. When the latter shock reaches the outer free boundary of the case it reflects as a rarefaction, accelerating the case outward and driving a rarefaction back into the liquid in B. After multiple reflections in C, the

agent and case achieve a common outward velocity. This expansion of the case induces hoop stresses which eventually cause it to fracture. From this point on, spherical symmetry is destroyed and the behavior of the system becomes very difficult to describe. Filler B is ultimately dispersed in droplets throughout a volume the order of a thousand times its initial volume and then further dispersed by diffusion and convection in the atmosphere. Various steps in the early process are illustrated in Figs. 9.13 and 9.14.

In Fig. 9.13 is shown the effect of a uniform shock wave in the agent, B as it impinges on the outer case, C. The case is assumed to have higher impedance than B, as shown in Fig. 9.13 (b). The points labelled 1, 2, 3, . . . in Fig. 9.13b correspond to the regions 1, 2, 3, . . . in Fig. 9.13a. The states 3, 5, 7, . . . are all zero pressure states corresponding to the condition that the outer region is a void. The final velocity, u_f, is reached by the ringing up process shown. In practice the incident shock is not uniform but is followed by a rarefaction with states lying along OC in Fig. 9.13b. This means that the states 4, 6, 8, etc. do not lie on a single cross curve of material C as shown, but on a succession of cross curves, each lying below the previous one. Then the final velocity is less than u_f and is reached in a time which depends on the rate of decay of the wave behind the initial shock. Clearly it takes a longer time to reach the final state if OC is very steep.

In Fig. 9.14 is illustrated the somewhat more complicated situation at the inner shell, A. Here again it is assumed that the incident wave is a uniform shock and the geometry is plane. To take the real situation into account is straightforward but tedious. The final state reached in this case is found just as in the previous problem, but instead of ringing up to states along the $p = 0$ axis, the material in A rings up to u_f on the Hugoniot of B, which is assumed here to lie below A. Here, too, the effect of the rarefaction following the incident shock or detonation wave is to replace the single cross-curve 1, 2, 4, . . . by others lying successively below one another until a final state

to the left of u_f is reached on OB.

The analyses shown in Figs. 9.13 and 9.14 are reasonably applicable to a burster in which the cases are very thin. Then the rise time associated with ringing up can be ignored. Otherwise the more complicated analysis taking account of rarefactions as indicated above is required.

Although it is helpful to break the problem into pieces and analyze these by characteristic methods, any detailed calculations are better done by direct numerical integration using a Q-code of the kind described in Chapter 5. Such calculations are useful in describing the early stages of burster behavior, but they are useless beyond the point of fragmentation of the outer shell. Then considerations beyond those discussed in this book control the situation and, in fact, the later behavior is very poorly understood.

9.4.2 Penetration of Armor by Projectiles

Protection of a target by armor and penetration of armor by projectiles are very complicated problems, and their complete understanding requires much more in the way of mechanical and physical consideration than is the subject of this book. However, impact and shock do play major roles in the process of penetration, and by using the concepts developed in preceding chapters we can gain some understanding of the process.

First of all we note that there are three possible modes of failure for any armored target. The one which predominates when large, slow projectiles impinge on it is structural failure. In the case of a simple plate this occurs initially by bending, then by stretching and, finally, fractures may occur. At high velocities penetration is controlled by local impact effects without involvement of bending or gross structural failure. Roughly speaking this will occur when the time required for the projectile to penetrate the target is small

compared to the time for a bending wave to reach the nearest support member. At intermediate velocities, both local and structure effects are important. The third mode is spall, associated usually with direct attack by explosive in contact with the armor, although it may result also from high velocity projectile impact: if a layer of explosive of thickness 1/16 to 1/2 the thickness of steel armor plate is placed in contact with the plate and detonated, a layer of thickness the order of half the explosive thickness or greater and of area somewhat less than the explosive area will be rippled off and projected inward at high velocity. The mechanisms of spall have been disucssed by Rinehart [9.33] and others and will not be considered here.

Low velocity penetration is apt to be controlled by bending, as indicated above. In a simple approximation we can suppose that the plate is subjected only to membrane forces and is supported at radius c. If the target has been stressed to its yield point, σ_o, then the force resisting penetration is

$$F_1 \simeq \sigma_o \pi dh \sin\theta \simeq \sigma_o \pi dh\, x/c \tag{9.12}$$

where d, h, x, c are defined in Fig. 9.15. Then if perforation of the plate occurs at displacement x_o, the energy required for perforation is

$$W_1 \simeq \pi \sigma_o dch\, (x_o/c)^2 \tag{9.13}$$

Equating this to the kinetic energy of the projectile having mass m, we get for the minimum velocity for perforation,

$$v_c = 2\sqrt{\pi \sigma_o dh/m}\; x_o/\sqrt{c} \tag{9.14}$$

At somewhat higher velocities the force resisting penetration will be augmented by shear resistance of the plate itself. In Fig. 9.16 we envision a situation in which penetration of the target is achieved by the projectile pushing out a plug of the same diameter. We again suppose that the target is stressed

to the failure point σ_o and that the shear represents a drag stress acting on the projectile:

$$F_2 = \pi d \sigma_o x \, . \tag{9.15}$$

The work done in pushing out the plug is

$$W_2 = \pi d \sigma_o h^2/2 \, . \tag{9.16}$$

Adding Eqs. (9.13) and (9.16) yields the expression

$$\frac{W}{d} = \frac{W_1 + W_2}{d} = S(hc + ah^2) \tag{9.17}$$

where $S = \pi\sigma_o(x_o/c)^2$ and $a = c^2/2x_o^2$. Supposing that $\sigma_o x_o/c$ is a constant of the target material, we find that Eq. (9.17) yields a reasonable representation of the threshold energy required to penetrate steel plates up to 0.3 inches thick with flat ended rods for W/d up to 1500 ft-lbs/inch [9.34]. This is within the range of incidence one might expect for reactor control rods ejected by accident and incident on the protecting shell of the reactor complex. If the projectile is very long, the time required for penetration of the target may not be large compared to the time for a wave to travel from one end of the projectile to the other. In that case it is appropriate to match the wave impedance of the rod to that of the plate instead of considering it a rigid mass. For example, suppose the rod is infinitely long and penetration is resisted by a force $F(x)$. Then the resistance generates a simple wave in the rod, and the equation of motion becomes

$$dx/dt = u_o - \sigma/\rho v = u_o - 4F(x)/\pi d^2 \rho v \tag{9.18}$$

For $F(x)$ given by $F_1 + F_2$ in Eqs. (9.12) and (9.15), this yields

$$x = (u_o/a)\,[1 - \exp(-at)] \tag{9.19}$$

where $a = 4\sigma_o(1 + h/c)/d\rho v$

ρ = density of projectile

v = speed of thin bar waves in projectile

u_o = initial velocity of projectile

If u_o is sufficiently large, $x = x_o$ for finite t and the projectile penetrates with some residual velocity. Fig. 9.17 is a micrograph of a target which has not been completely penetrated by a projectile. Both the shearing out of the plug and bending of the target are evident.

At still higher velocities complete perforation of a thin target may be easily achieved, but the velocity of the projectile is significantly reduced. This reduction can be estimated from the forces of Eqs. (9.12) and (9.15) and from momentum exchange with the target. As projectile velocity increases, momentum exchange dominates and the final velocity can be calculated simply by equating the initial momentum of the projectile with the final momentum of projectile plus a plug from the target having the same area as the projectile. Then the velocity loss for initial velocity v_o is

$$\Delta v/v_o = \alpha/(1 + \alpha) \tag{9.20}$$

where $\alpha = \rho Ah/m$

ρ = target density

A = cross section of projectile

h = target thickness

m = projectile mass .

The principal mechanism of energy absorption for slow projectiles is probably plastic bending of the target plate. On impact a plastic bending wave radiates outward and the radius affected after a time t is proportional to $\sqrt{t}$. As projectile speed increases, time for penetration decreases and the plate area

subject to bending gets smaller. Thus bending becomes less important as projectile speed increases. From these concepts, one can understand why pointed projectiles penetrate more easily than flat ended ones. As the pointed end penetrates into the target it generates bending waves, but these bending waves travel outward at a slower rate than the projectile radius increases, therefore the mechanism of bending is removed or effectively reduced as a source of energy absorption.

So far we have been discussing ideal situations in which the projectile is undeformed by the impact and subsequent penetration. This approximation is reasonably accurate up to velocities of a few thousand feet per second at most, and it may fail well below a thousand feet per second. Sir Geoffrey Taylor has described the process of projectile distortion for flat-ended steel projectiles on armor plate [9.35]. By allowing the impact to generate elastic-plastic waves in the projectile, with elastic waves reflecting between the plastic wave front and the rear of the projectile, he was able to describe mushrooming of the projectile at a few hundred feet per second. At the order of a thousand feet per second the approximations in his theory failed as distortion became more extreme. In general it can be assumed that the contact area between projectile and target will be increased by plastic distortion.

At velocities of six to ten millimeters per microsecond hydrodynamic behavior of both projectile and target can be invoked. Then the penetration procedure becomes analogous to digging into the earth with a garden hose: a hole is "washed" in the target and the projectile is consumed in the process. The mechanics of jet penetration, treating both projectile and target as incompressible fluids was first developed during World War II [9.36]. When applied to a semi-infinite target as in Fig. 9.18, the theory yields depth of penetration, d, in terms of the projectile or jet length, L:

$$d = L\sqrt{\rho_j/\rho}$$

where ρ_j = density of jet material and ρ = density of target material. This theory has been widely used in connection with shaped charges and is reasonably successful for ductile materials with high melting points. It does not work well for glass or for lead.

At extremely high projectile velocities, say 50 mm/μsec, new phenomena come into play. A small pellet striking a thick target can be expected to come to rest very quickly and at a short distance into the target. Its total energy has been given to the target in this time and is confined to a volume bounded by the stopping time and the shock propagation velocity. The latter limit expresses the inability of the target material to carry energy away from the impact point as rapidly as it is delivered. Consequently the energy density in the target may be very high; much higher, for example, than in a chemical explosive, so the effect of the impact on the target is the same as a very intense, nearly point explosion.

In this discussion of penetration an effort has been made to describe the kinds of physical and mechanical behavior which can be expected in various material and velocity regimes. The formulae given are at best approximate, but the idea that penetration results from competition between mechanisms for carrying energy away from the impact point and rate of delivery of energy in impact is sound. Unfortunately, implementation of this idea is not simple.

It has been tacitly assumed, for the most part, that both projectile and target are ductile. If they are brittle, crack propagation must be added as a mechanism for energy transport. ~~The problem is somewhat more complicated but not fundamentally altered.~~

The penetration problem is not fundamentally changed in this case, but effects on both projectile and target can be dramatic because of the large Hugoniot elastic limits and compression moduli which can be obtained in brittle materials. This is well illustrated by a program being carried on at the Livermore Lawrence Laboratories by Mark L. Wilkins and his colleagues[9.37~9.41]. They are concerned with the penetration of ceramic-faced two-component armor by small-caliber projectiles with impact velocities from about 1000 to 3000 ft/sec. They have conducted parallel numerical and experimental studies which have led to a new understanding of the penetration process and to new concepts in armor design.

The geometry of their experiments is shown in Fig. 9.19. Some significant features of a typical calculation are shown in Fig. 9.20. There the dark regions radiating from the point of impact and growing from the interface toward the projectile represent regions of fracture. This work deals almost exclusively with ceramic materials which have large Hugoniot elastic limits and large compression moduli. Consequently the stress developed at the point of impact is very much greater than the yield strength of the projectile, causing it to flow laterally and to be essentially removed from further consideration. While this destruction of the projectile tip is occurring, the fracture conoid shown in Fig. 9.20 is spreading toward the interface of ceramic and the backup plate. The backup plate itself is subjected to a large pressure over an area approximately defined by the extension of the fracture conoid, and as a result of this pressure there is a strongly localized movement of the interface away from the impact surface. This

movement arises from a combination of material compression under the impact point, deformation produced by strong shearing stresses caused by the non-uniform loading, and bending response of the backup plate. The initial deflection produces tension in the ceramic near the interface. The ceramic is weak in tension, so it fractures in the region adjacent to the interface and beneath the impact point.

As time passes the region of fracture spreads to encompass the entire fracture conoid, the local compression modulus is reduced so that the impact stresses lie below the yield stress of the projectile, deterioration of the projectile tip is arrested and the penetration proceeds. The ceramic turns out to retain its effective modulus well beyond the time when fracture is complete within the fracture conoid. For the case shown, fracture is nearly complete at six microseconds after impact, but projectile erosion continues for approximately 9 more microseconds. The net result of this is that only about 60% of the projectile energy is delivered to the target. The rest of it is carried away by the ejecta.

Dramatic evidence of the correctness of the above ideas is contained in a series of experiments in which ceramic thickness, backup thickness and materials were varied. Some of the most germane are briefly described below.

(i) 0.34" of Al_2O_3 (Coors Ad-85 Alumina) was backed by a one inch plate of tool steel. A projectile striking it at 2300 ft/sec was completely destroyed and, except for a few cracks in the ceramic, radiating from the impact area, the target was intact and undamaged. Here the axial fracture region resulting from plate motion was suppressed, so the compressive modulus of the ceramic remained high.

(ii) Aluminum backup plate thickness, S, was varied while ceramic thickness, Δ, was held constant. The ballistic limit, V_{BL}, increased steadily with S until $S \simeq 0.23"$*. At this thickness there was a nearly discontinuous increase in V_{BL}, and for larger S, V_{BL} increased only slowly. This change results from a transition of backup plate response from the bending mode for thin plates to shear or plug fracture, like that shown in Fig. 9.17, for thick plates.

(iii) Ceramic thickness, Δ, was varied while backup plate thickness was held constant. It was found that V_{BL}/Δ was constant for any particular ceramic. The numerical value of the constant depends on the ceramic material and on the dynamic strength of the backup material. Surprisingly, the dynamic strengths of 6061-T6 Al and woven fiberglass roving turn out to be nearly the same, though their bending moduli are much different. The constancy of V_{bl}/Δ is suggested by the following simple argument. Suppose that the ceramic responds elastically to impact even at these high pressures. Then the stress produced at any point in the ceramic is proportional to impact velocity and decreases approximately with distance, r, from the point of impact as 1/r. Then at the ballistic limit the stress at the ceramic-backup interface is proportional to V_{BL}/Δ. The constancy of V_{BL}/Δ implies that motion of the interface is the primary reason for failure of the target to defeat the projectile, and that this motion depends upon the stress applied to the backup plate.

*V_{BL} is the impact velocity at which the probability of penetration is 0.5.

(iv) Simultaneous measurements were made of positions vs time of rear surface of the projectile, projectile-ceramic interface, ceramic-backup interface, and back face of the Al backup plate using flash x-rays and streak camera. From these it is evident that erosion of the projectile continues until almost twenty microseconds after impact and that penetration into the target does not start until about that time. In this particular case the projectile velocity was 2800 ft/sec and the residual length of the projectile, after erosion was complete, was 0.55 inches. With a fiberglass backup plate, penetration started earlier, perhaps as early as ten microseconds, and erosion of the projectile continued until almost 30 microseconds, though the final length was the same as for aluminum backup. This difference is apparently due to the lower bending modulus of fiberglass.

(v) Geometric scaling was verified for Coors Ad-85 Alumina, B_4C and BeO ceramic targets using 0.25", 0.30" and 0.45" projectiles. When target dimensions were changed in the same ratio, V_{BL} was unchanged, indicating that the penetration process does not depend significantly on dynamic effects such as dislocation moetion, and that it does not involve any characteristic physical lengths.

(vi) The effects of projectile strength were verified by experiments in which the projectile was both "stronger" and "weaker" than the target. If the projectile is stronger, it goes through the target with but little deformation. If it is weaker, it erodes in the fashion described above, and it makes little difference how much weaker. In this context, "stronger" means having a larger compression modulus, a larger Hugoniot elastic limit and a larger yield strength in tension. The relative

importance of these is ill-defined. If the projectile is weaker than the ceramic, penetration seems to depend primarily on the kinetic energy of the projectile.

From the above discussion it is clear that a high ballistic limit for a two component armor requires a ceramic with high compressive strength and modulus which will resist tensile stresses, perhaps because of ductility, at the ceramic-backup interface. The backup plate should have a high bending modulus and strength and a high shear strength. Since fiberglass and aluminum backup give similar results, it is apparent that the ability to withstand large deflections compensates in some way for lack of bending stiffness. Since V_{BL}/Δ is constant for a given ceramic, it is clear also that lightweight ceramics are advantageous because Δ is larger for a given weight and V_{BL} is thus increased.

A search for new materials, including beryllium-boron compounds, is underway and it is apparent that this detailed study will lead to significant improvements in armor.

The computations described above were made with the two dimensional "HEMP" Code [9.42]. There are a number of other two dimensional codes which are suitable for these problems; all require a great deal of machine time for detailed analysis.

Chapter 9

LIST OF SYMBOLS

A	area
c	sound speed
d	thickness
D	detonation velocity
F	force
m	mass
N	the number of moles of gas
P	pressure
Q	heat of reaction
r	radius
R	Universal gas constant
t	time
T	temperature (p. 2), transit time (p. 16)
u	particle velocity
U_p	particle velocity
U_s	shock velocity
v	speed
V	specific volume
α	draf coefficient
γ	ratio of specific heat
ρ	density
σ_o	yield stress

LIST OF FIGURES

Figure 9.14 Idealized behavior at inner shell boundary.
(a) x-t plane , (b) p-u plane

Figure 9.15 Low velocity penetration

Figure 9.16 Shear resistance to penetration

Figure 9.17 Micrograph of 1/4" steel target partially penetrated by 1/4" diameter steel sphere. Target Material - 4130 tempered martensite. Projectile - 2100 steel at 1.2d mm/μsec. Courtesy of Marvin E. Backman, USN Ordnance Station, China Lake, California.

Figure 9.18 Penetration of semi-infinite target by high velocity jet. v = jet velocity, U = penetration velocity

Figure 9.19 Geometry of the (LLL) experiments. In some cases the projectiles were .25" and .45" diameter.

Figure 9.20 Calculation of development of fracture conoid and axial crack in alumina. [9.39]

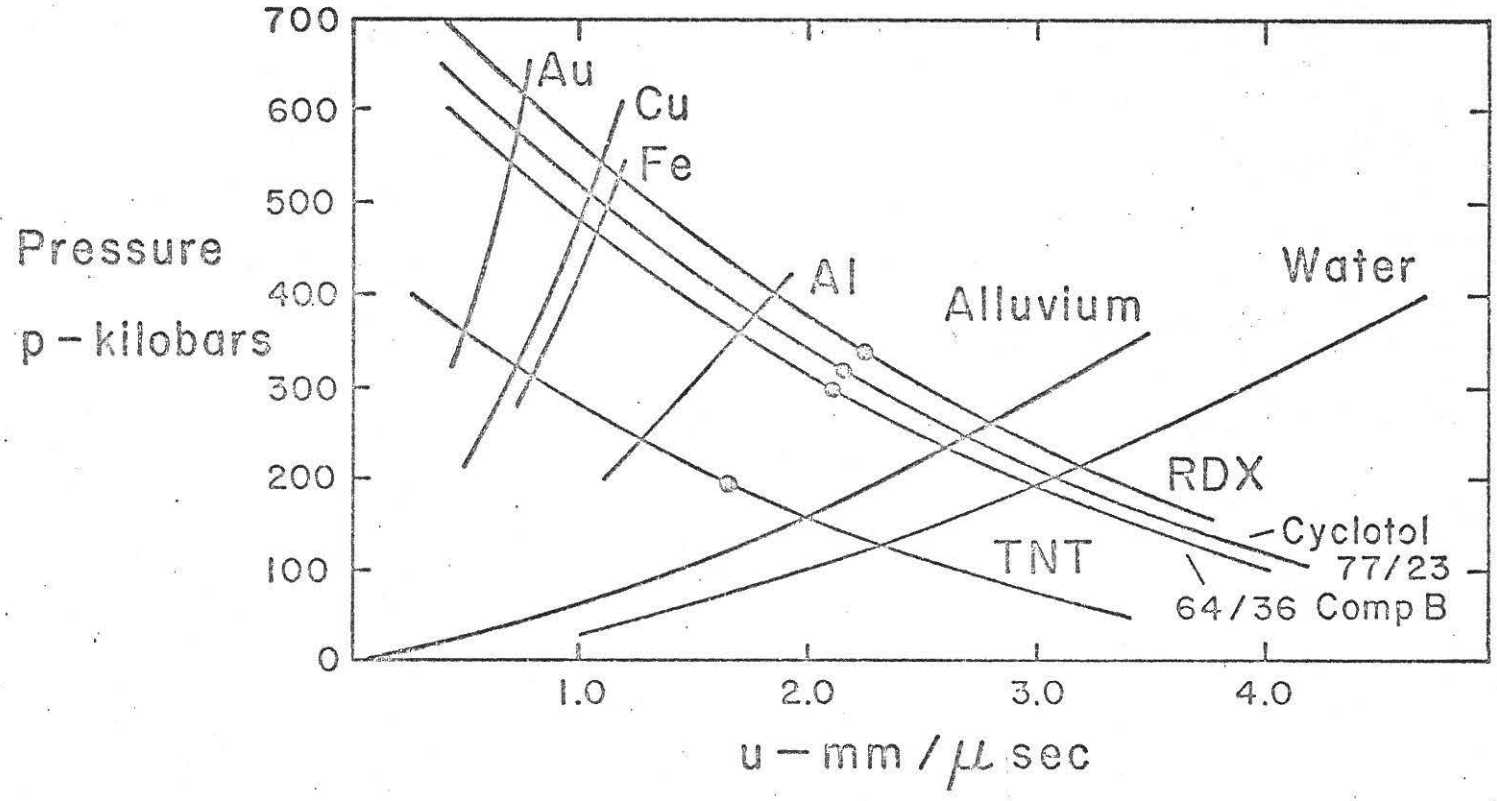

Fig 9.1 Shock wave velocities in high explosives

Figure No. 9.1 "Duvall"

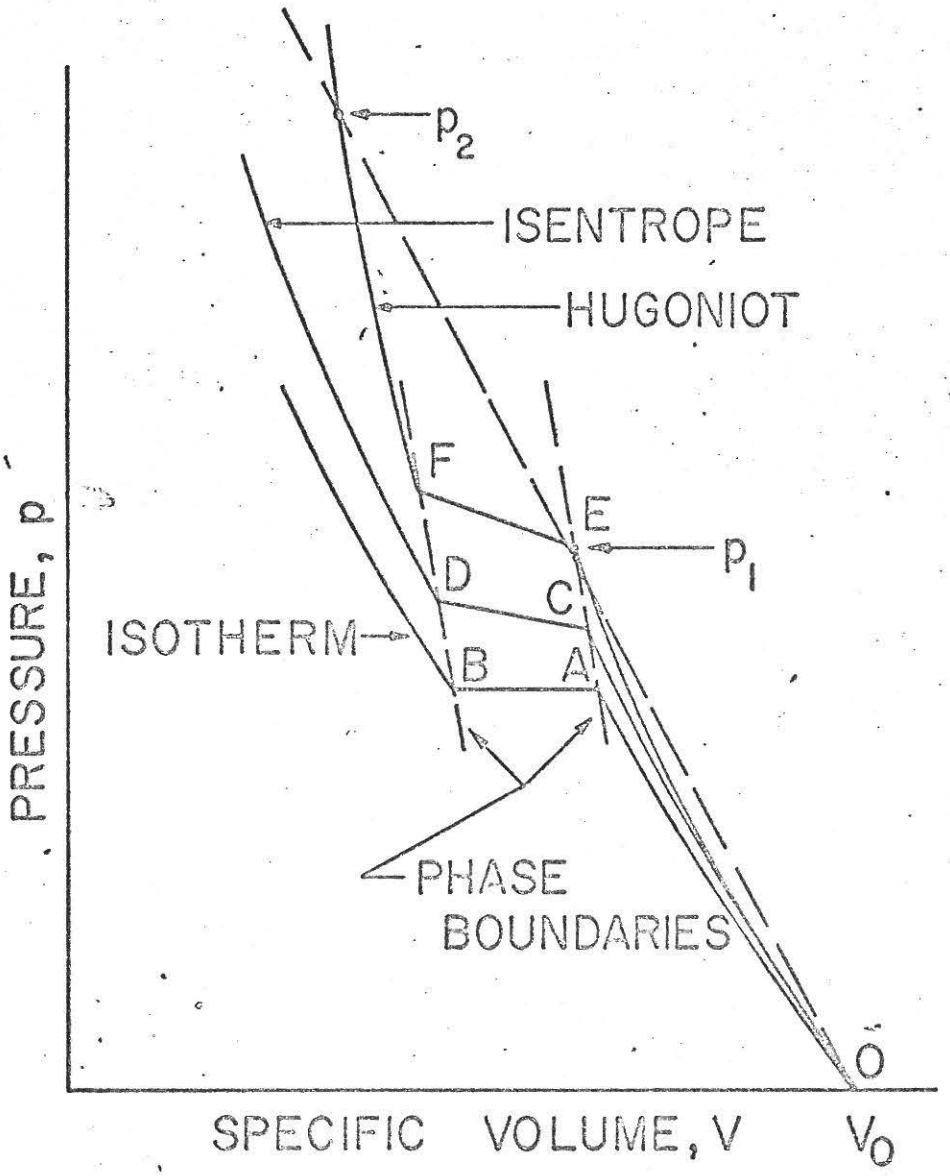

Figure No. 9.2 "Duvall"

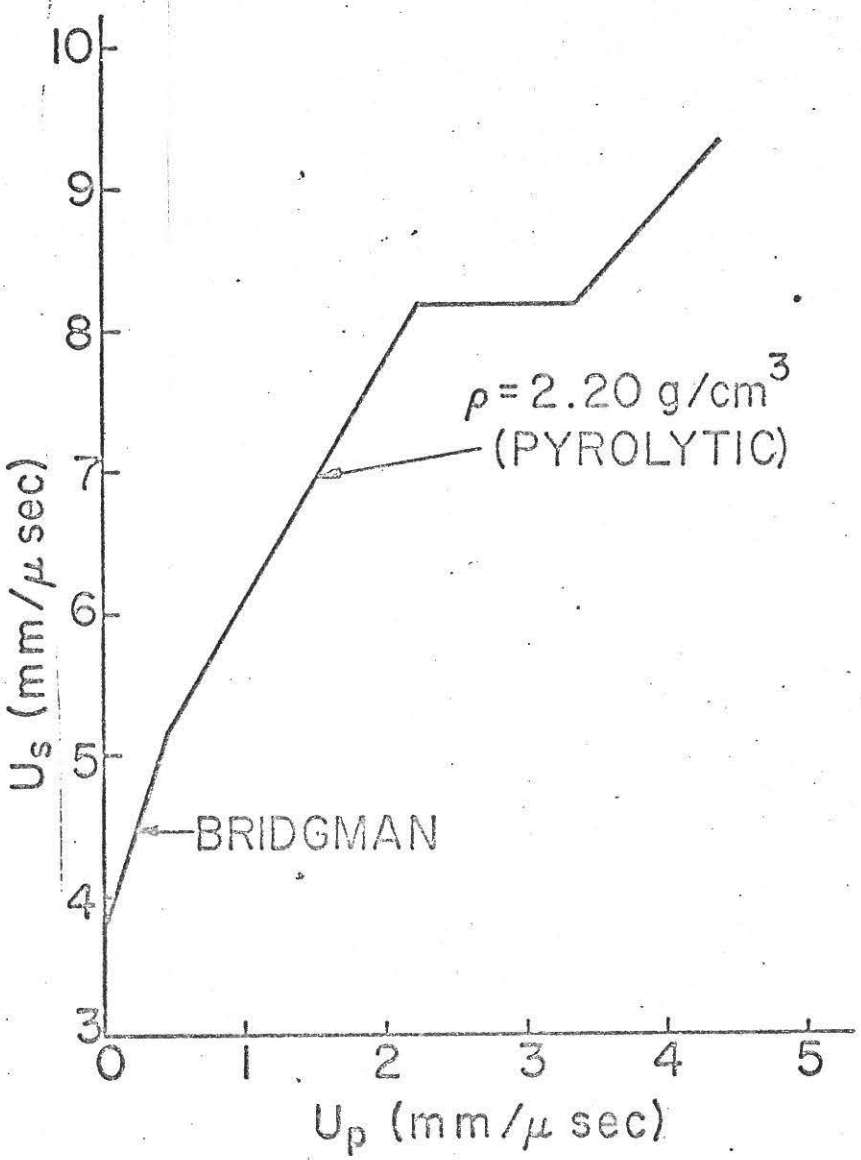

Figure 9.3 "Duvall"

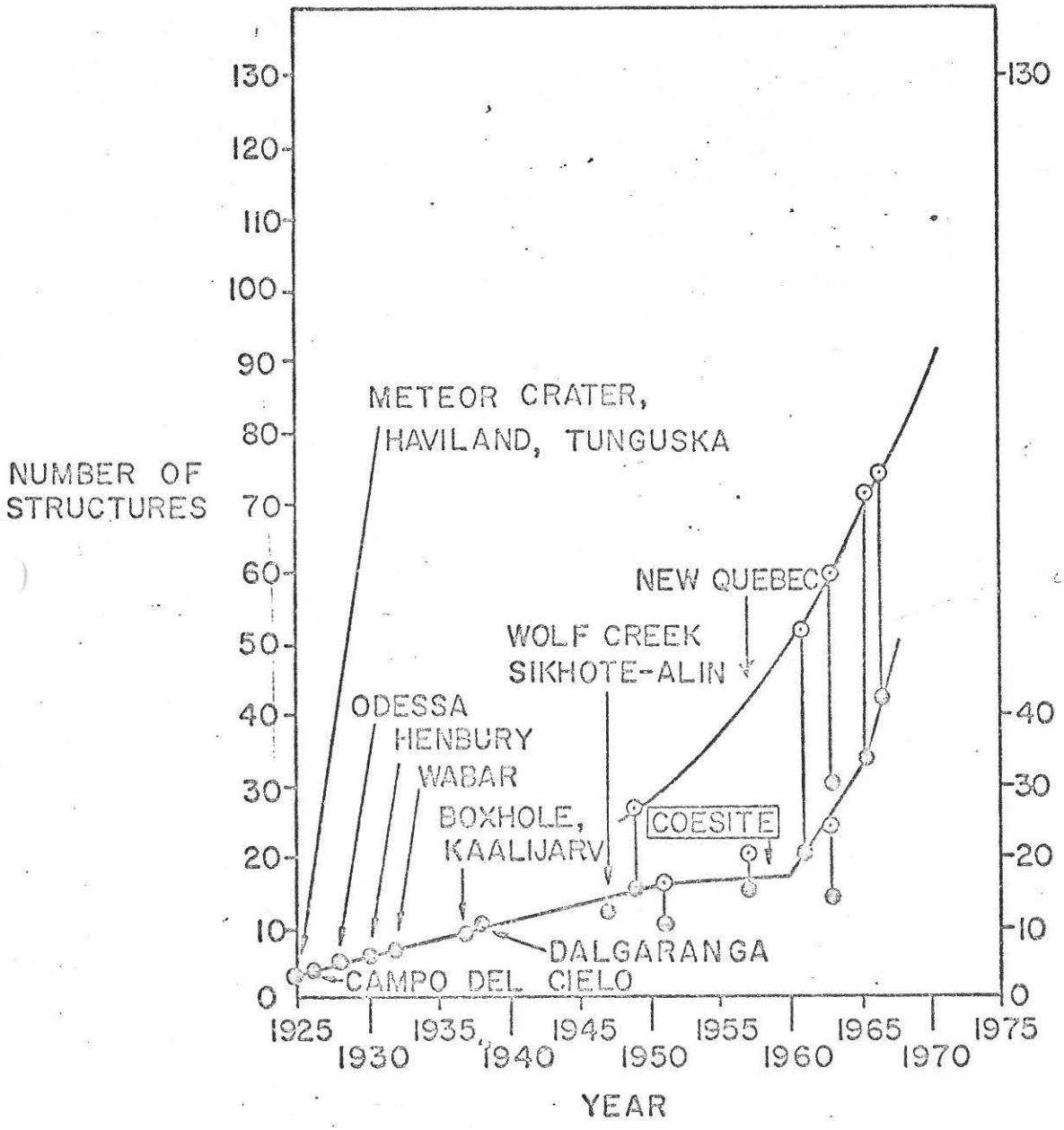

Figure No. 9.4 "Duvall"

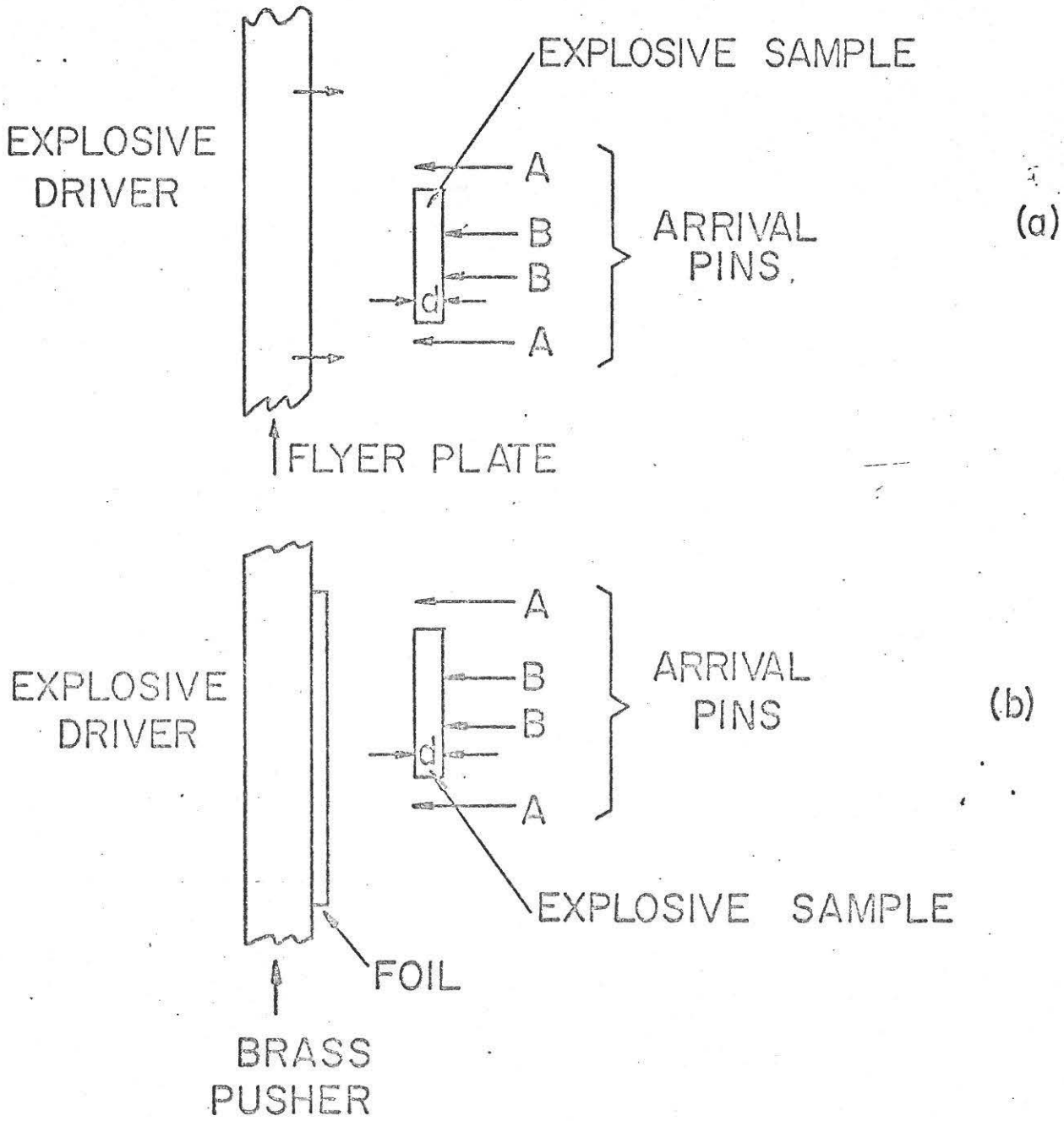

Figure No. 9.5 "Duvall"

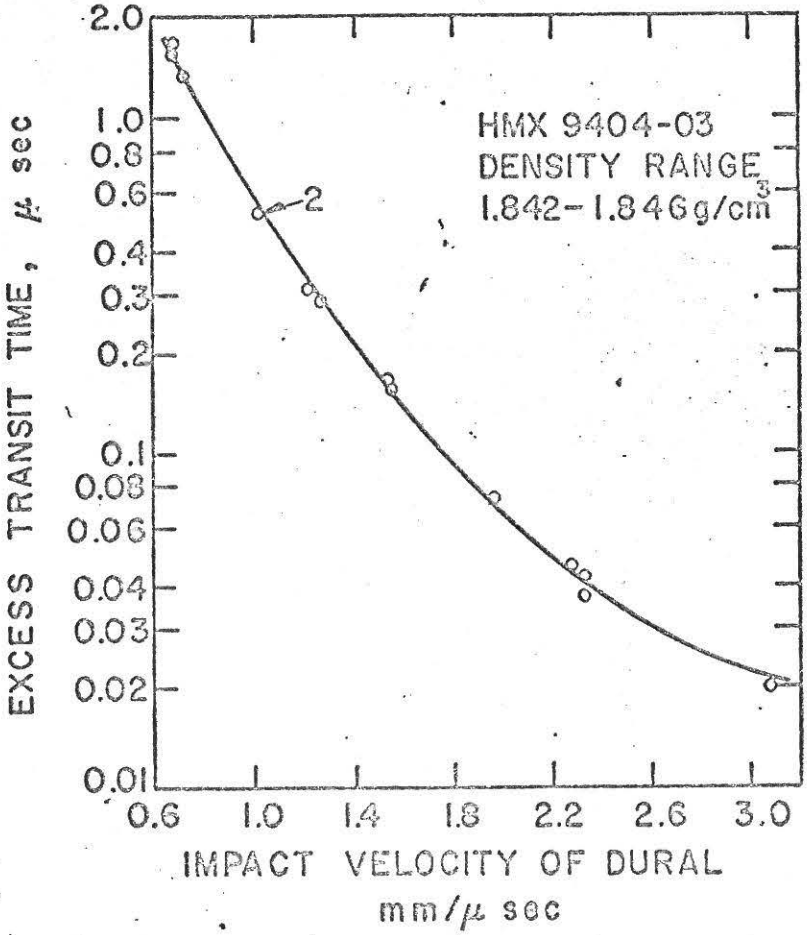

Figure No. 9.6 "Duvall"

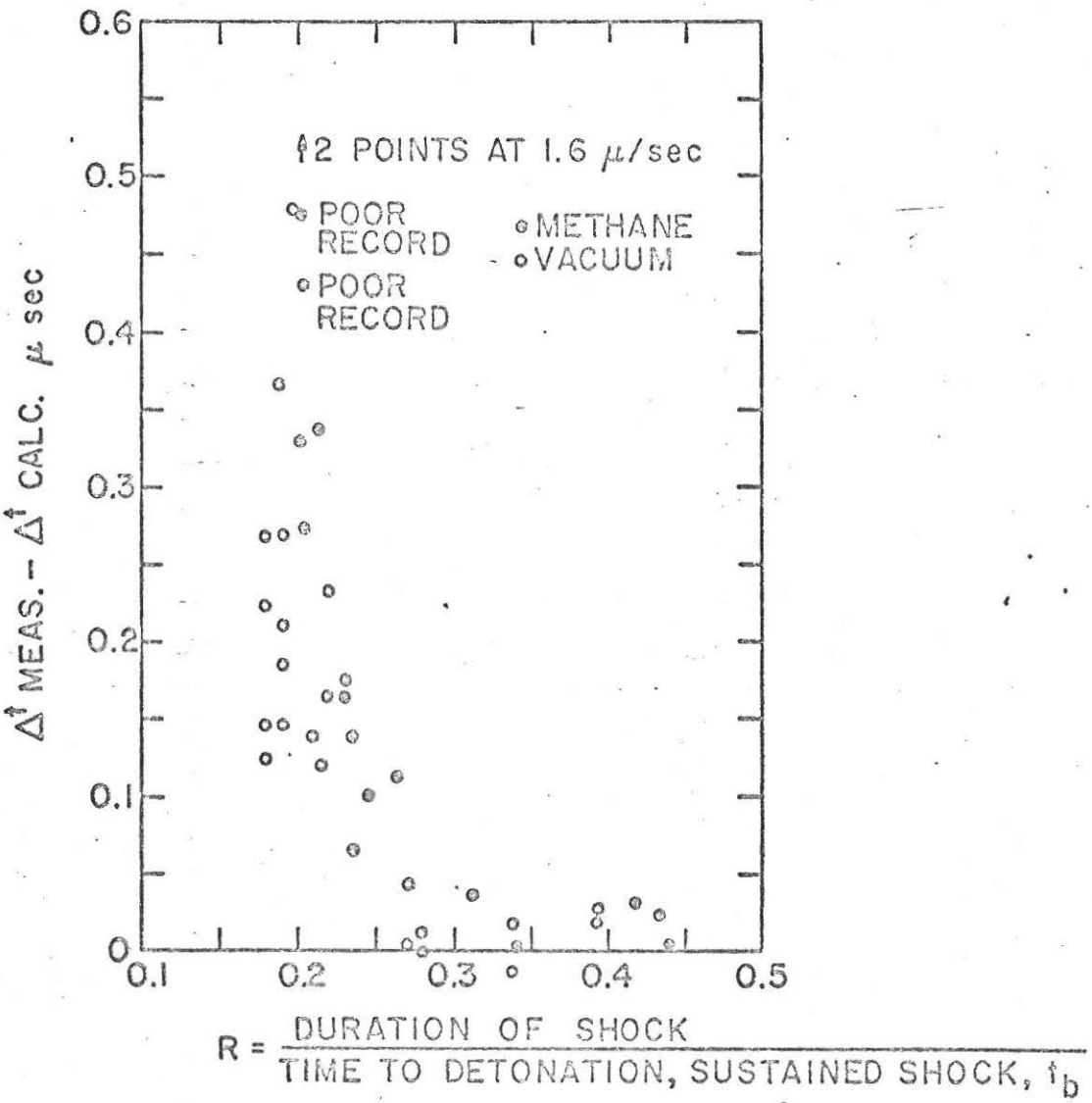

Figure No. 9.7 "Duval

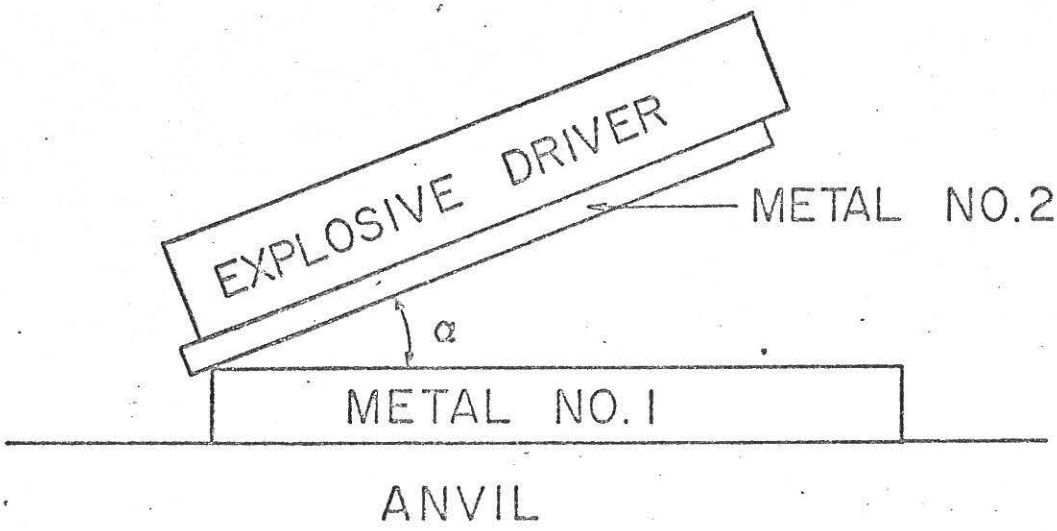

Figure No. 9.8 "Duvall"

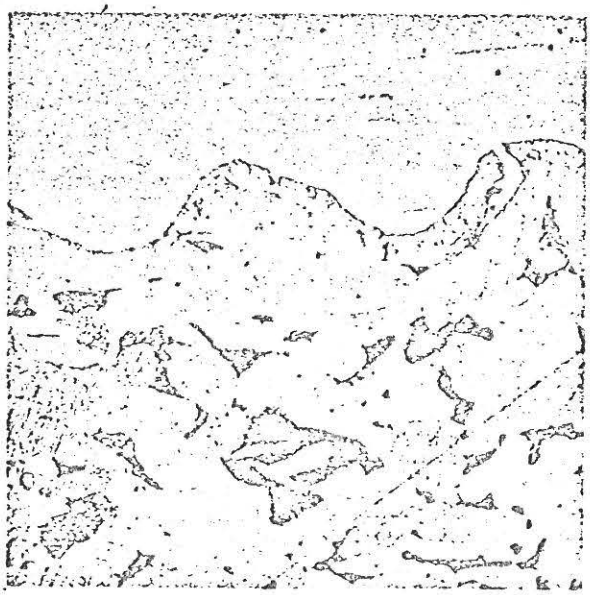

STEEL–Ni

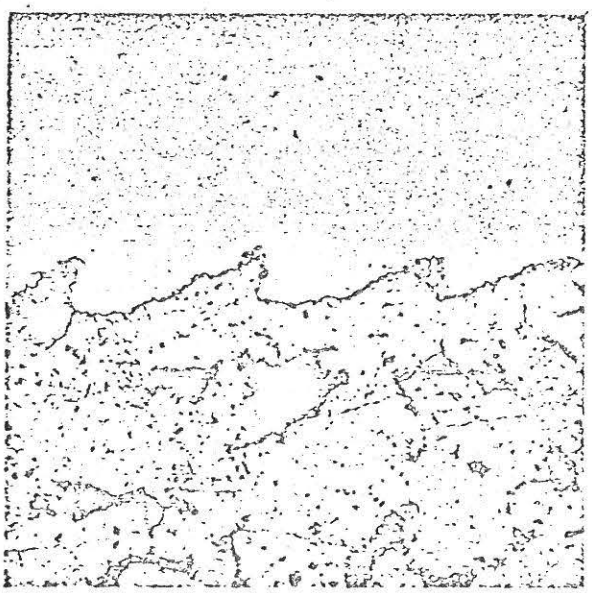

STEEL–Mo

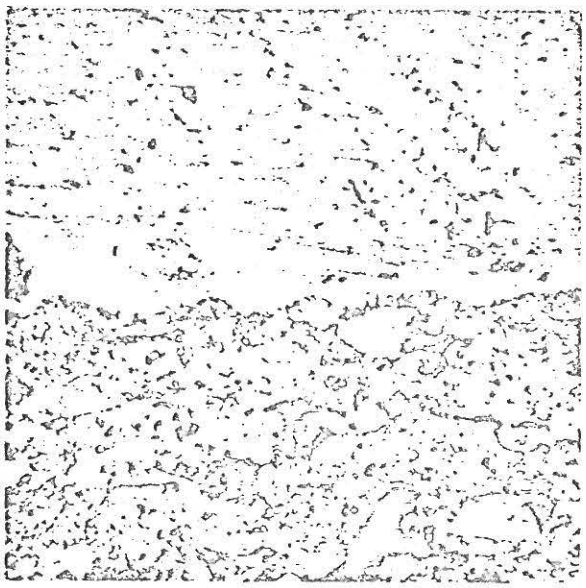

STEEL–Nb

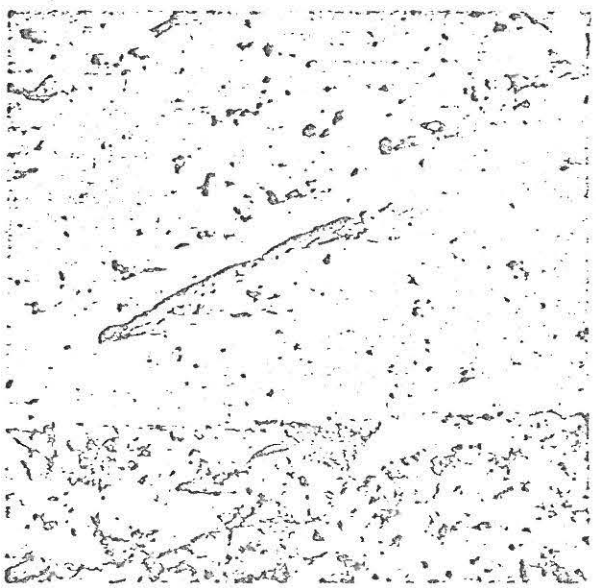

STEEL–Ti

Fig 9.9

Micrographs of impact bonds formed from the configurations of Fig 9.8 (obtained through the courtesy of Standard Research Institute)

(Return this page to SRD)

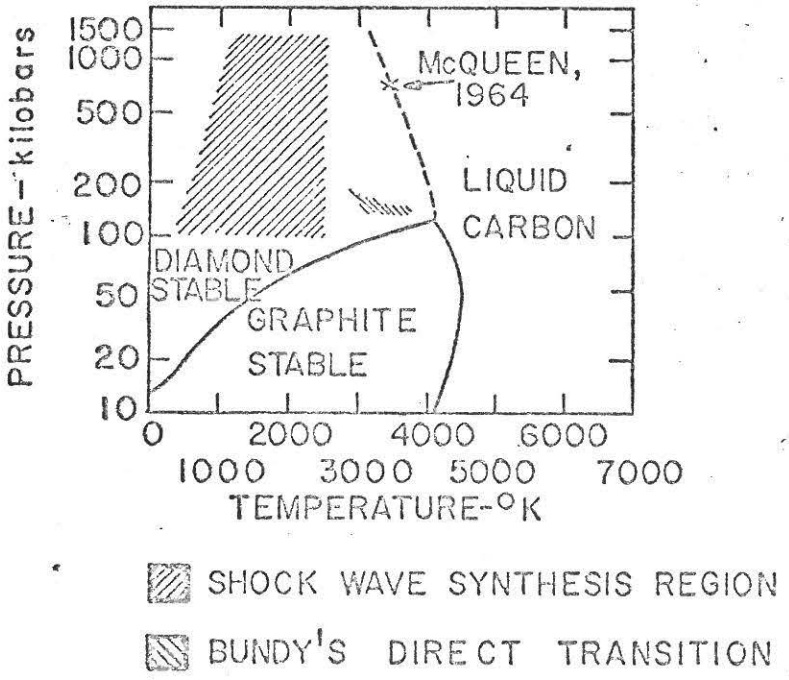

Figure No. 9.13 "Duvall

owner of the De Carli patent, US 3,238,019. Allied Chemical is presently offering for sale diamonds synthesized by the shock wave technique described and claimed in this patent[25].

Although we do make very small diamonds by shock wave synthesis, we are by no means limited to the production of small diamonds. We have in fact produced polycrystalline diamonds of nearly a millimetre in diameter similar in appearance to the meteoritic diamonds described by Carter and Kennedy. I have photographed some of these large diamonds, all of which measure 500 to 700 microns in their largest dimensions (Figures 1, 2 and 3). In some of these particles one may observe veins

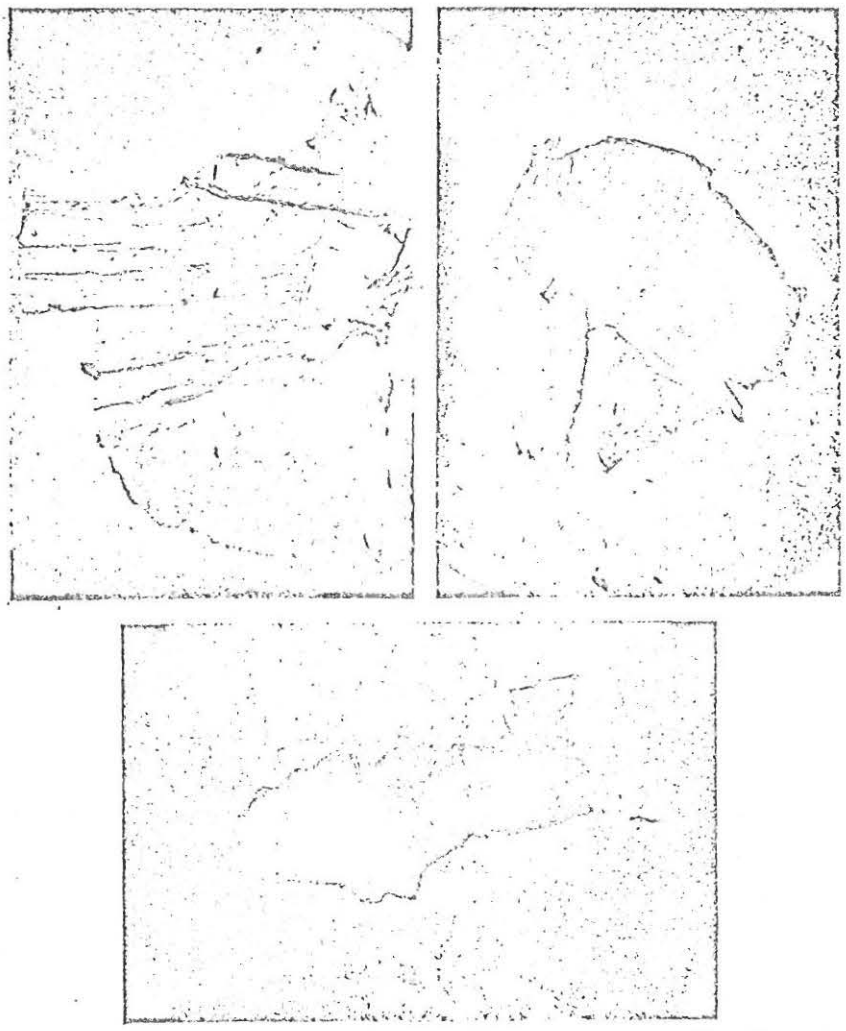

FIGURES 1, 2, 3. Shock wave synthesized diamonds. These polycrystalline diamonds are 500 to 700 microns in their longest dimensions although they are only about 10 microns thick

FIG 9.11

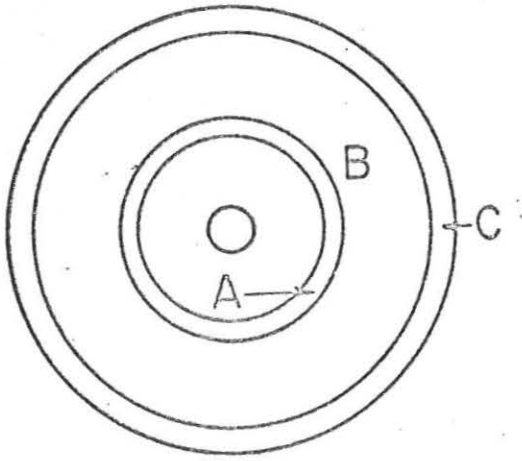

Figure No. 9.12 "Duvall

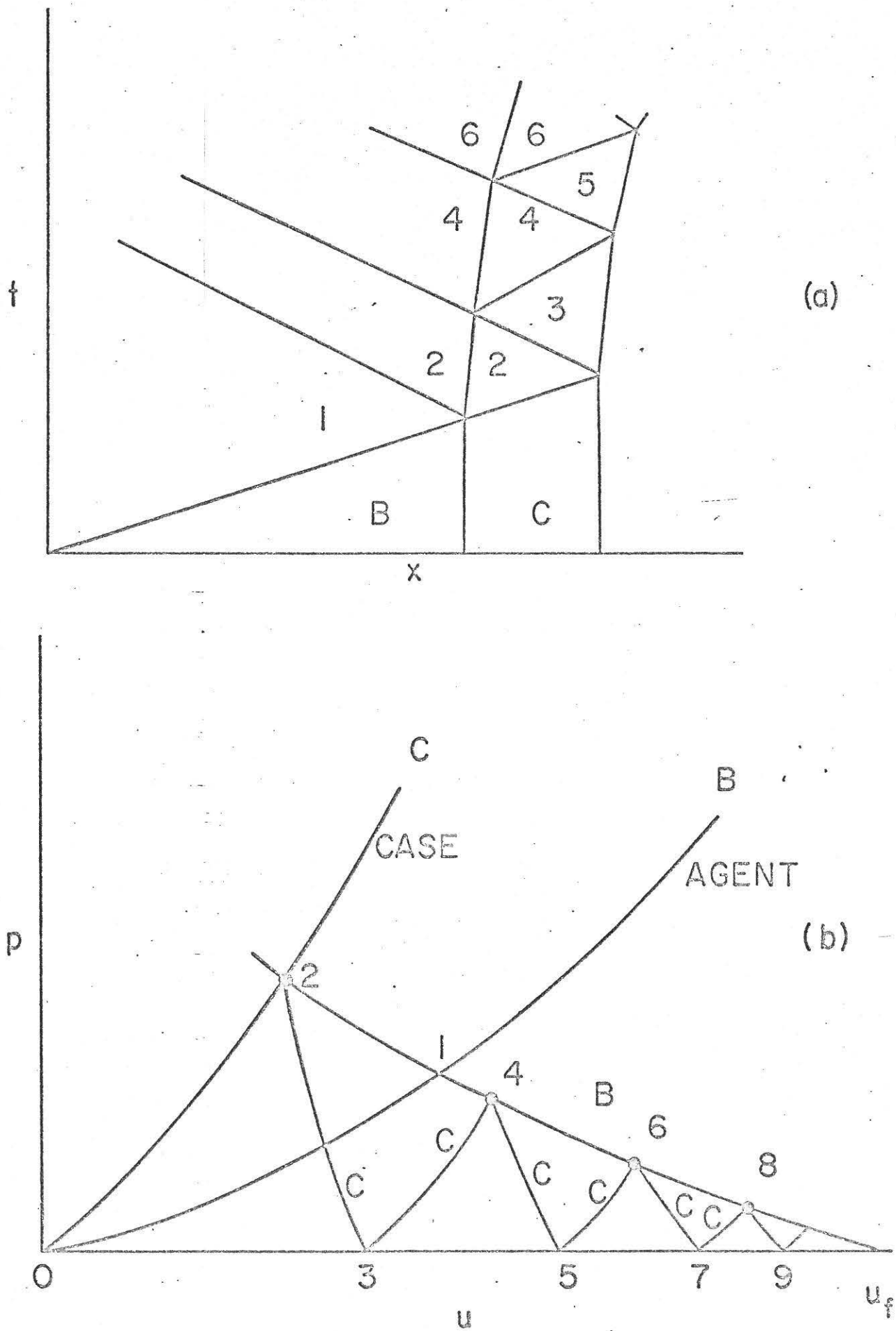

Figure No. 9.13 (a) & (b)

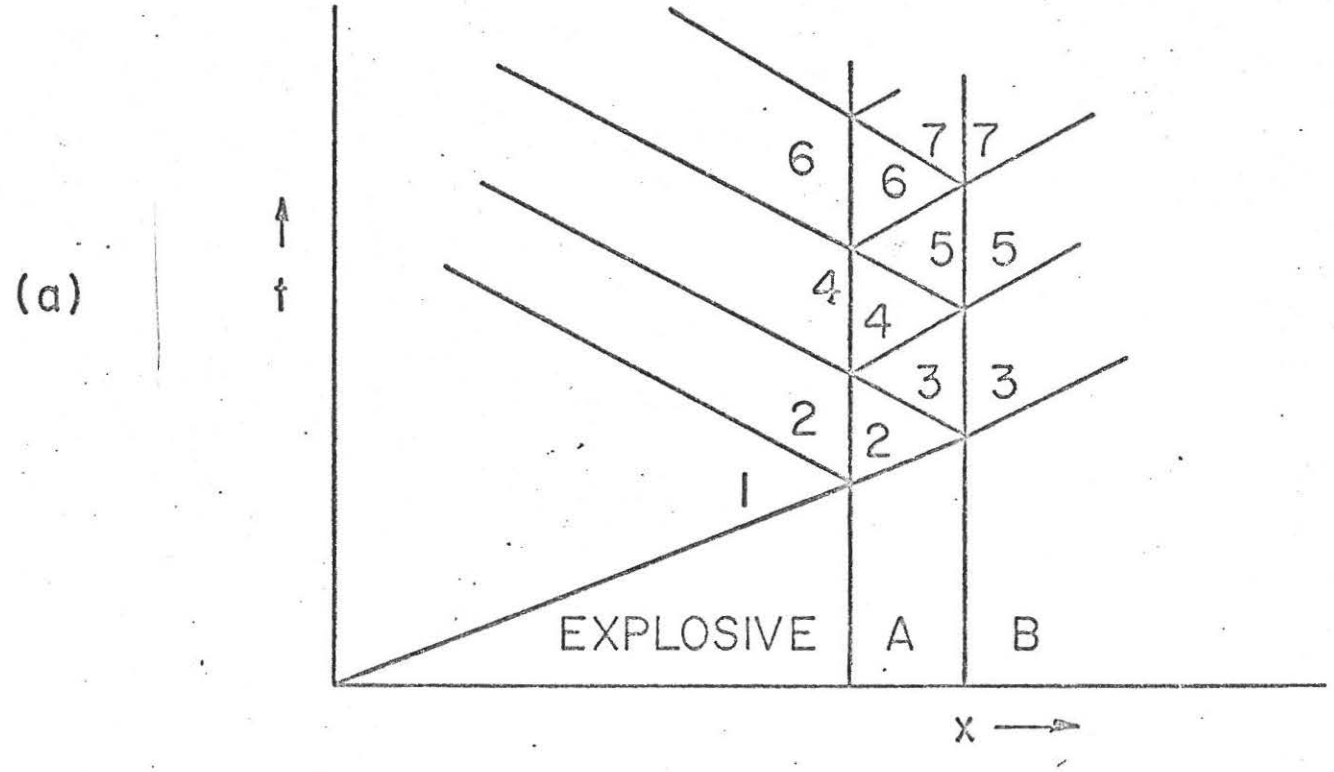

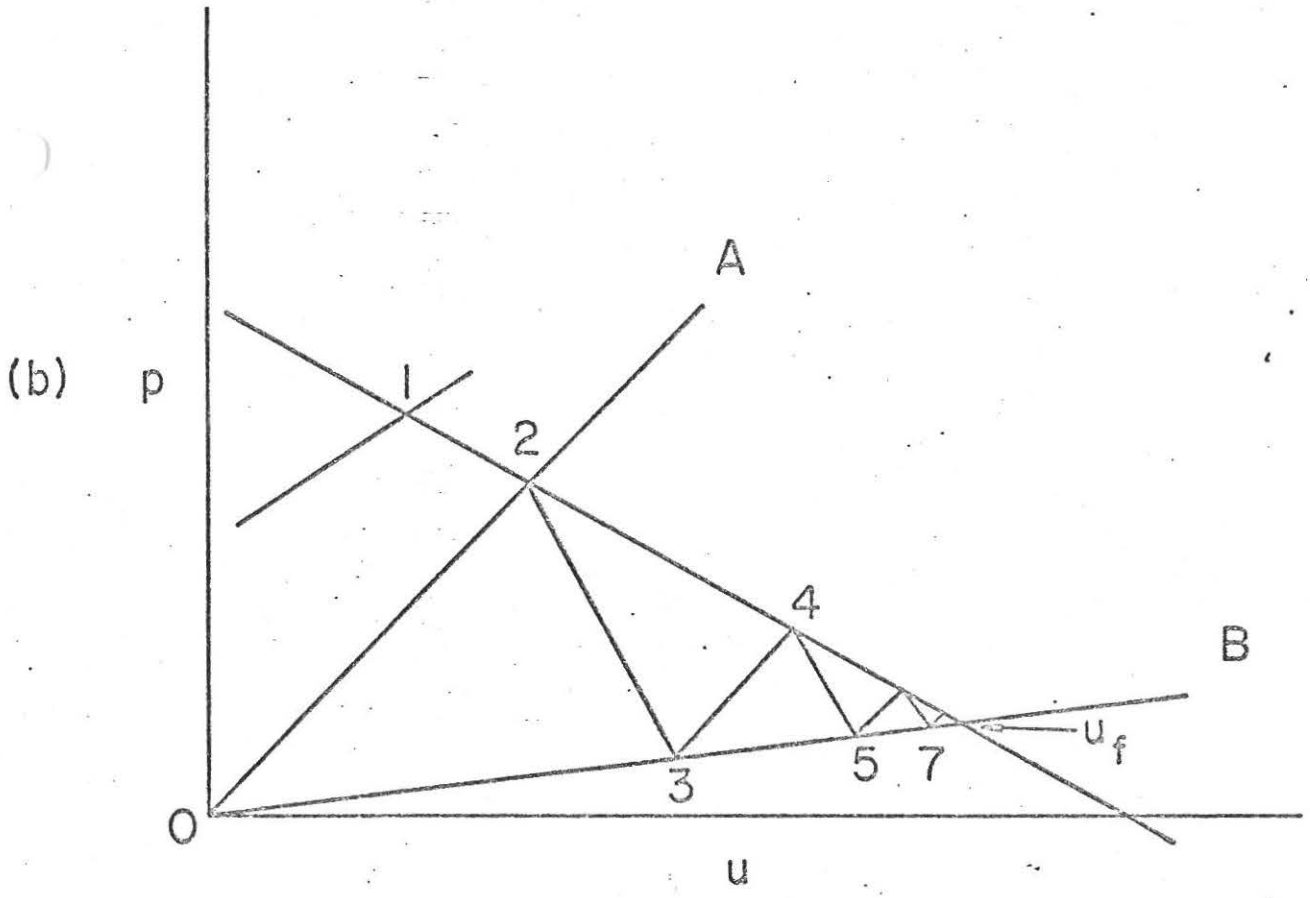

Figure No. 9.14 "Dunn

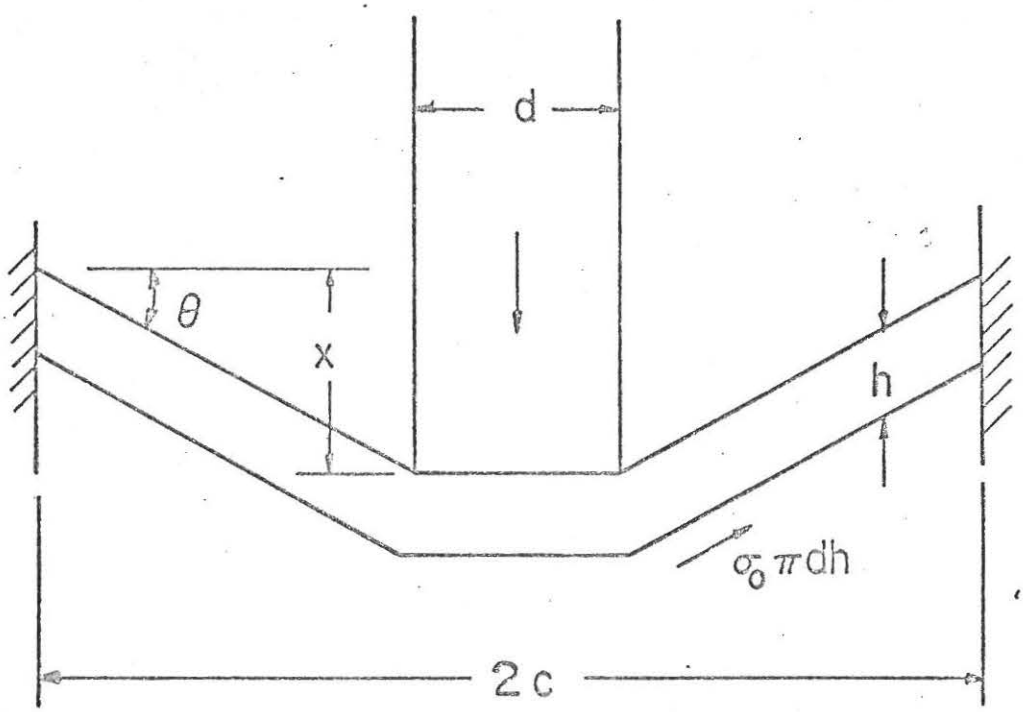

Figure No. 9.15 "Duvall"

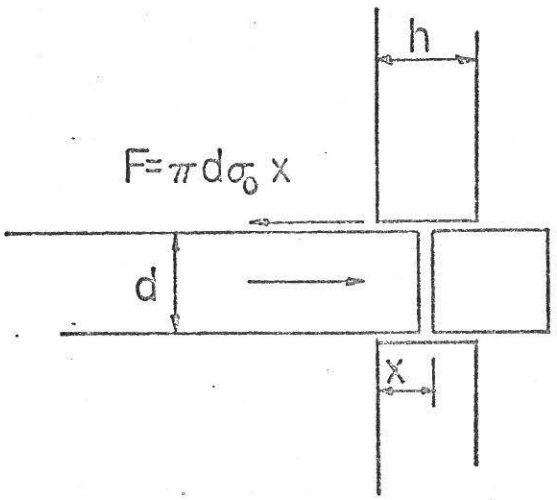

Figure No. 9.16 "Duvall"

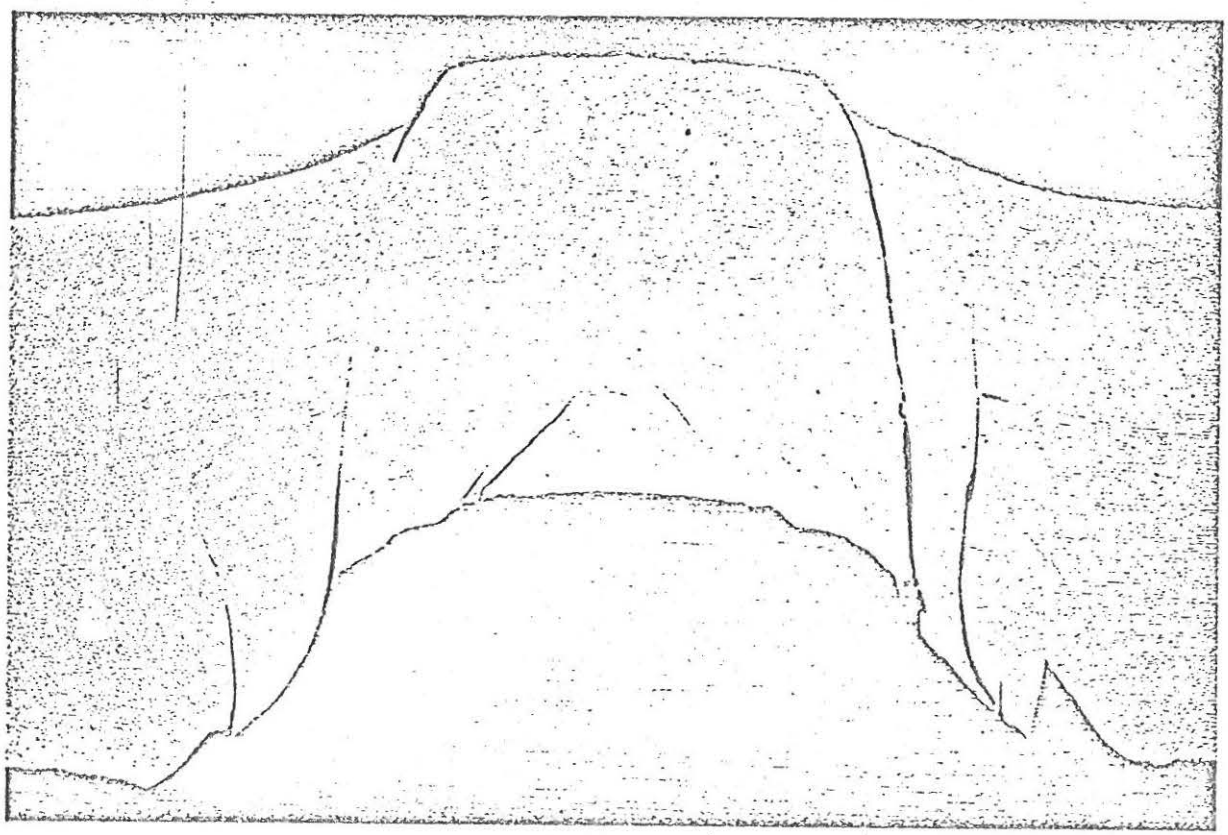

Fig 9.17

1/4" steel

Micrograph of target partially penetrated by 1/4" steel sphere. Target material - 4130 tempered martensite. Projectile material - 52100 steel at 1.24 mm/μsec. Courtesy of Marvin E. Backman, USN Ordnance Station, China Lake, Calif.

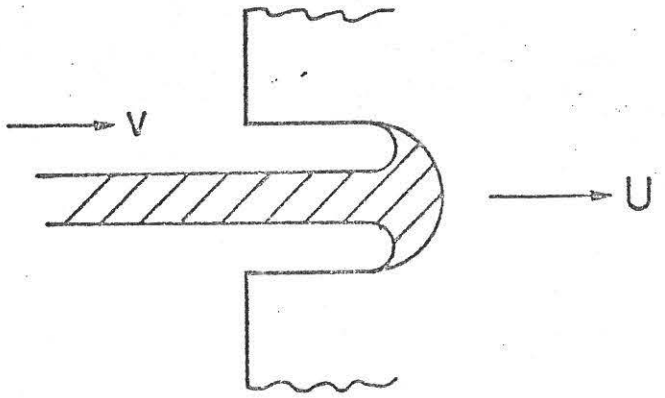

Figure No. 5.18 "Duvall"

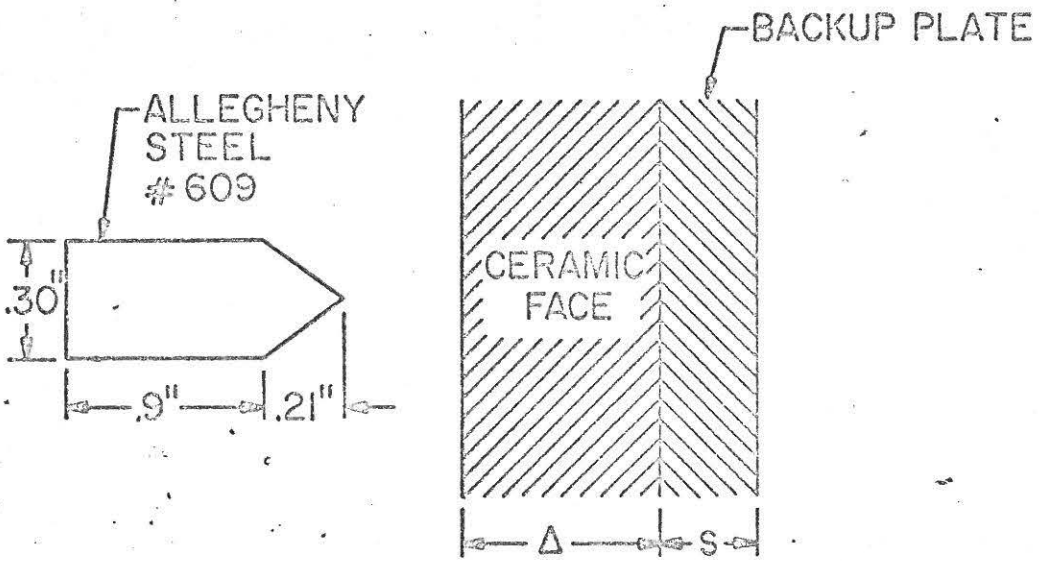

Fig. 9.19

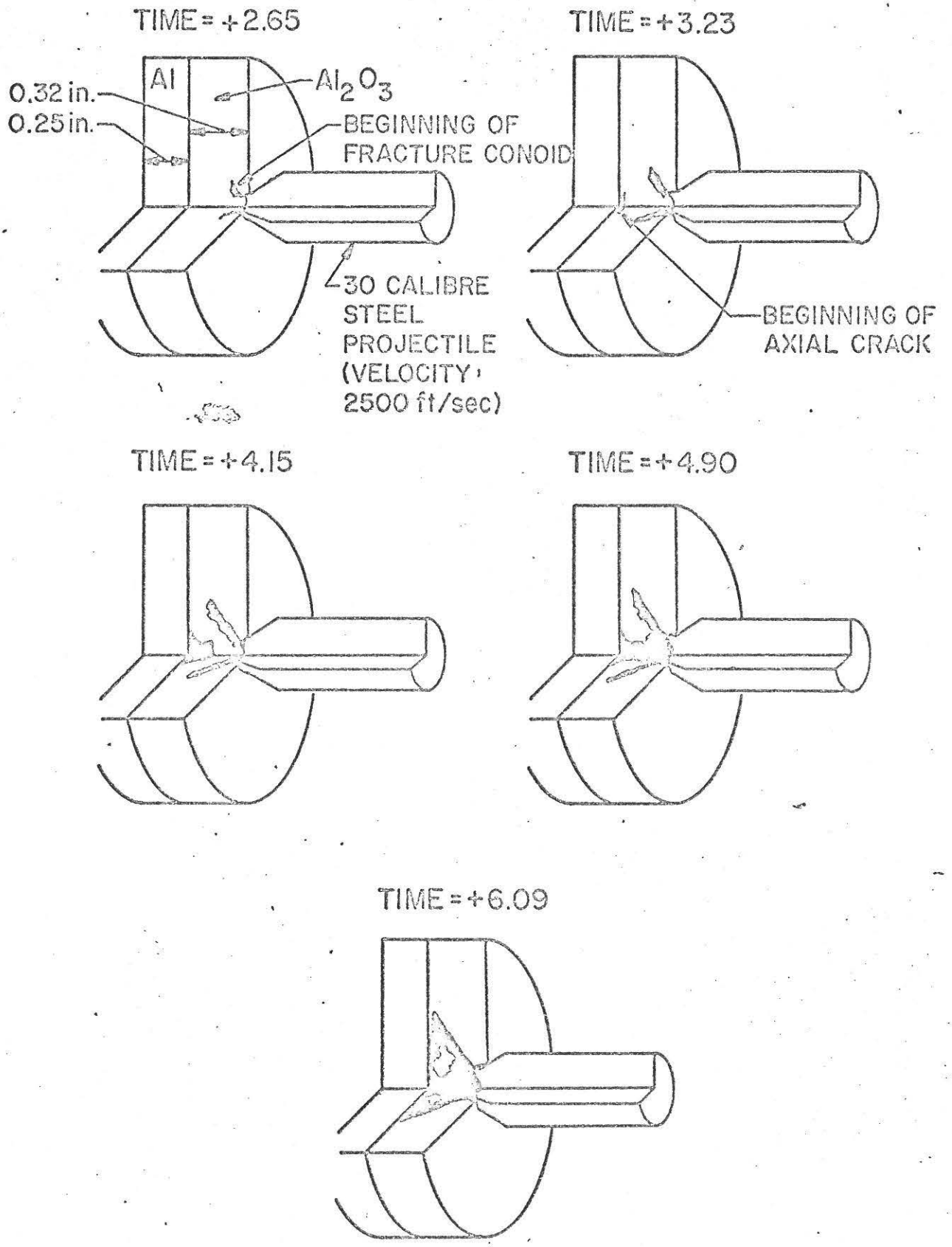
TIME = +2.65
Al
Al_2O_3
0.32 in.
0.25 in.
BEGINNING OF FRACTURE CONOID
30 CALIBRE STEEL PROJECTILE (VELOCITY, 2500 ft/sec)
TIME = +3.23
BEGINNING OF AXIAL CRACK
TIME = +4.15
TIME = +4.90
TIME = +6.09

Fig. 9.20

Chapter 9.

REFERENCES

9.1 Taylor, J., "Detonation in Condensed Explosives," Oxford, 1952.

9.2 "Proceedings Fourth Symposium (International) on Detonation" Oct. 12-15, 1965, U. S. Naval Ordnance Lab., White Oak, Md. ACR-126 Office of Naval Research--Dept. of the Navy, Washington, D.C. Supt. of Doc., U.S. Govt. Printing Office, Wash., D. C., 20402.

9.3 Berger, J. and Viard, J., "Physique des Explosif Solides," Dunod, Paris, 1962.

9.4 Minshall, Stanley, "Investigation of a Polymorphic Transition in Iron at 130 kb," Bull. APS, Vol. 29 (12/28/54), p. 29 (A).

9.5 Johnson, P. C., Stein, B. A., and Davis, R. S., "Temperature Dependence of Shock-Induced Phase Transformations in Iron," J. Appl. Phys., Vol. 33, pp. 557-561, February 1962.

9.6 McQueen, R. G., "Laboratory Techniques for Very High Pressures and the Behavior of Metals Under Dynamic Loading," Chap. 3 of "Metallurgy at High Pressures and High Temperatures," Gordon and Breach, 1964, edited by K. A. Gschneidner, Jr., M. T. Hepworth and N. A. D. Parlee.

9.7 Loree, T. R., Fowler, C. M., Zukas, E. G., Minshall, F. S., "Dynamic Polymorphism of Some Binary Iron Alloys," J. Appl. Phys., Vol. 37, p. 1918, 1966.

9.8 McQueen, R. G., Marsh, S. P., and Fritz, J. N., "Hugoniot Equation of State of Twelve Rocks," J. Geophys. Res., Vol. 72, No. 20, (10/15/67), pp. 4999-5036.

9.9 Larson, D. B., "A Shock-Induced Phase Transformation in Bismuth," J. Appl. Phys., Vol. 38, No. 4, pp. 1541-1546 (15 March 1967).

9.10 Alder, B. J. and Christian, R. H., Discussions of the Faraday Society, No. 22, p. 44-46, 1956.

9.11 Duvall, G. E. and Fowles, G. R., "Shock Waves," Chap. 9 of "High Pressure Physics and Chemistry," Vol. 2, Academic Press, 1914, R. S. Bradley, Ed.

9.12 De Carli, P. S. and Jamieson, J. C., "Formation of Diamond by Explosive Shock," Science, Vol. 133, p. 1821, 1961.

9.13 Duvall, G. E. and Fowles, G. R., loc. cit., pp. 285-286.

9.14 McQueen, R. G., Fritz, J. N., and Marsh, S. P., "On the Composition of the Earth's Interior," J. Geophys. Res., Vol. 69, pp. 2947-2965, 1964.

9.15 French, Bevan M., "Shock Metamorphism of Natural Materials," Mono Book Corp., Baltimore, 1968. Bevan M. French and Nicholas M. Short, Eds., pp. 1-18.

9.16 Thomas, R. N. and Charters, A. C., "Aerodynamic Performance of Small Spheres from Subsonic to High Supersonic Velocities," BRL Report No. 514, May 1, 1945. Ballistic Research Laboratories, Aberdeen Proving Ground, Md.

9.17 Lipschutz, M. E., "Shock Metamorphism of Natural Materials," Mono Book Corp., Baltimore, 1968. Bevan M. French and Nicholas M. Short, Eds., pp. 571-583.

9.18 Wood, John A., "Lunar Soil," Scientific American, Vol. 223, p. 14, August 1970.

9.19 Lunar Sample Preliminary Evaluation Team, "Preliminary Examination of Lunar Samples from Apollo 12," Science, Vol. 167, p. 1325 (3/6/70).

9.20 Gittings, Elizabeth F., "Initiation of a Solid Explosive by a Short Duration Shock," pp. 373-380, Proc. 4th Symposium on Detonation, U.S.N. Ordnance Lab., White Oak, Oct. 12-15, 1965. Published by U.S.N. Office of Naval Research as Report #ACR-126. Available from Clearinghouse for Federal Scientific and Technical Information, Springfield, Va., 22151, $5.00.

9.21 Ramsay, J. B. and Popolato, A., pp. 233-238, Op. Cit. (Ref. 9.20).

9.22 Davis, W. C. and Fickett, W., "Detonation Theory and Experiment," pp. 1-13 in "Behavior of Dense Media Under High Dynamic Pressures," Symposium H.D.P., I.U.T.A.M., Paris, Sept. 1967, Gordon and Breach, 1968.

9.23 "Proceedings of the Conference on Megagauss Magnetic Field Generation by Explosives and Related Experiments," EUR 2750.e, H. Knoepfel and F. Herlach (Eds.), Euratom, Brussels, 1966.

9.24 Davenport, D. E. and Duvall, G. E., "Explosive Welding," Creative Manufacturing Seminars, 1960-61, ASTME.

9.25 Walsh, J. M., Shreffler, R. G. and Willig, F. J., "Limiting Conditions for Jet Formation in High Velocity Collisions," J. Appl. Phys., Vol. 24, No. 3, pp. 349-359, March 1953.

9.26 Cowan, G. R. and Holtzmann, A. H., "Flow Configurations in Colliding Plates: Explosive Bonding," J. Appl. Phys., Vol. 34, No. 4, pp. 928-939, April 1963.

9.27 Sedykh, V. S., Deribas, A. A., Bichenkov Je. I., and Trishin, Yu. A., "Svarka Vzryvom," Svarochnoye Proizvodstvo, No. 5, pp. 3-6, 1962.

9.28 Sadwin, L. D., Illinois Institute of Technology Research Institute, Private Communication.

9.29 Wright, E. S. and Bayce, A. E., "Current Methods and Results in Explosive Welding," Stanford Research Institute, March, 1965. Presented at NATO Advanced Study Institute on High Energy Rate Working of Metals, Sandefjord/Lillehammer, Norway (September 1964).

9.30 De Carli, "Shock Wave Synthesis of High Pressure Phases; Comments on the Origin of Meteoritic Diamond" in Proc. Conf. on Industrial Diamonds, 1966, London, Industrial Diamond Information Bureau, 1967. J. Burls, Ed.

9.31 Crookes, W., "Diamonds", Harper, 1909.

9.32 De Carli, P. S., ASME Symposium on High Pressure Technology, December, 1970.

9.33 Rinehart, J. S. and Pearson, J., "Behavior of Metals Under Impulsive Loads," Am. Soc. Metals, Cleveland, Ohio, 1954.

9.34 Duvall, G. E., "Reactor Containment Work at SRI," Poulter Laboratories Internal Report 002-59, Stanford Research Institute, January 9, 1959.

9.35 Taylor, Sir Geoffrey, "Use of Flat Ended Projectiles for Determining Dynamic Yield Stress," Proc. Roy. Soc., A, 194, pp. 289-299, 1948.

9.36 Pugh, E. M., Taylor, Sir Geoffrey, Birkhoff, G., and MacDougall, D. P., J. Appl. Phys., Vol. 19, No. 6, pp. 563-582, June 1948.

9.37 Wildins, M. L., Honodel, C. A. and Sawle, D. R., "An Approach to the Study of Light Armor," Lawrence Radiation Laboratory, Livermore, California, Report UCRL-50284, June 13, 1967.

9.38 Wilkins, M. L., "Second Progress Report on Light Armor," LRL, Report UCRL-50349 (CRD), 1967.

9.39 Wilkins, M. L., "Third Progress Report on Light Armor," LRL, Report UCRL-50460, 1968.

9.40 Wilkins, M. L., Cline, C. F. and Honodel, C. A., "Fourth Progress Report of the Light Armor Program," LRL, Report UCRL-50694, June 4, 1969.

9.41 Wilkins, M. L., Landingham, R. L., and Honodel, C. A., "Fifth Progress Report of the Light Armor Program," LRL, Report UCRL-50980, January 1971.

9.42 Wilkins, M. L., "Methods in Computational Physics," Vol. 3, Academic Press, Inc., N. Y., 1964.

INTERNAL REPORTS - 1974

1. J.J. Dick, "Some Computer Programs", Internal Report 74-01, April, 1974.
2. Y.M. Gupta, Internal Report 74-02, July, 1974.